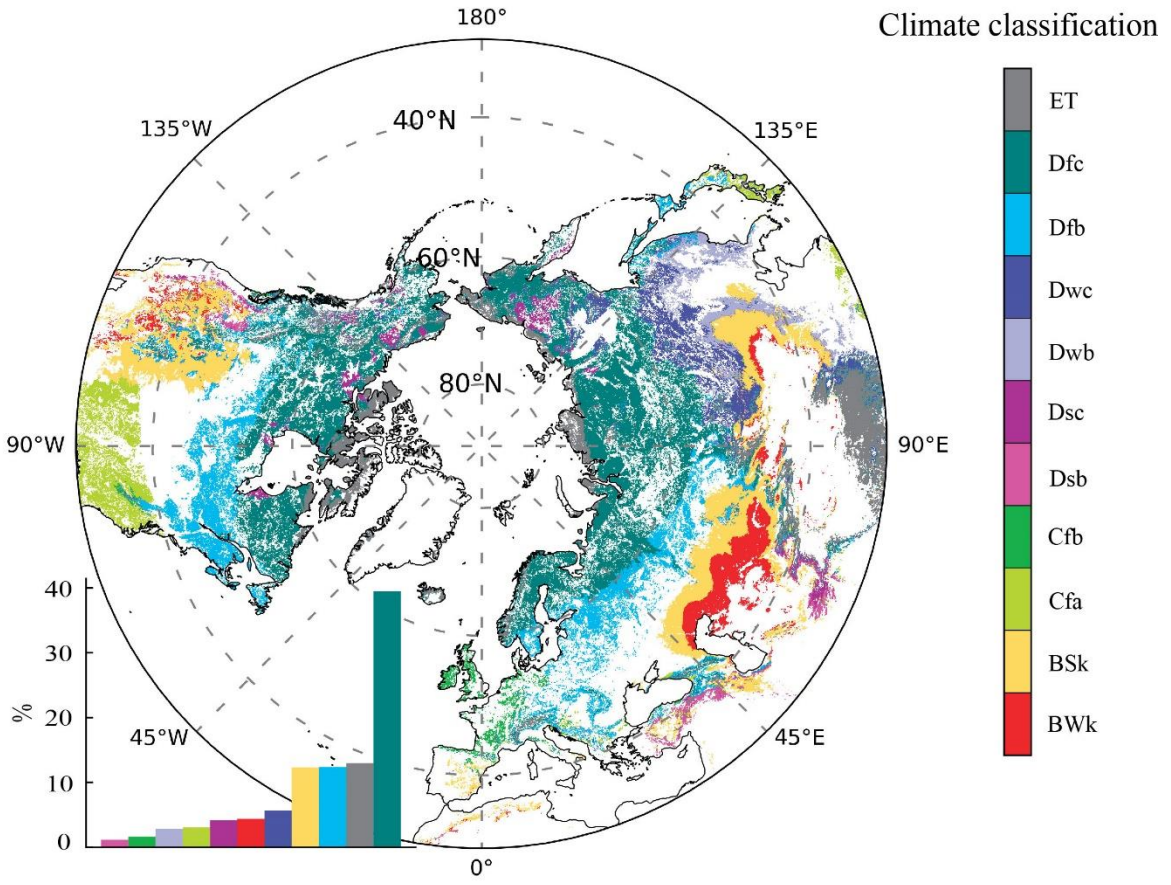


Figure S1: The spatial distribution of climatic types based on the latest Köppen-Geiger climate classification system in the middle and high latitudes of the Northern Hemisphere.

Table S1: The number of net ecosystem carbon exchange(NEE) sites based on different vegetation functional types

IGBP	Number of sites	Ratio (%)
1	492	38.2
2	15	1.2
3	21	1.6
4	40	3.1
5	6	0.5
6	3	0.2
7	30	2.3
8	553	42.9
9	70	5.4
10	59	4.6

Table S2: Spectral index formulas

Vegetation indices	Formulas
EVI	$\mathrm{EVI} = 2.5 \times [(\rho_2 - \rho_1)/(\rho_2 + 6 \times \rho_1 + 1.0 \times \rho_3 + 0.5)]$
NDSI	$\mathrm{NDSI} = (\rho_4 - \rho_5)/(\rho_4 + \rho_5)$

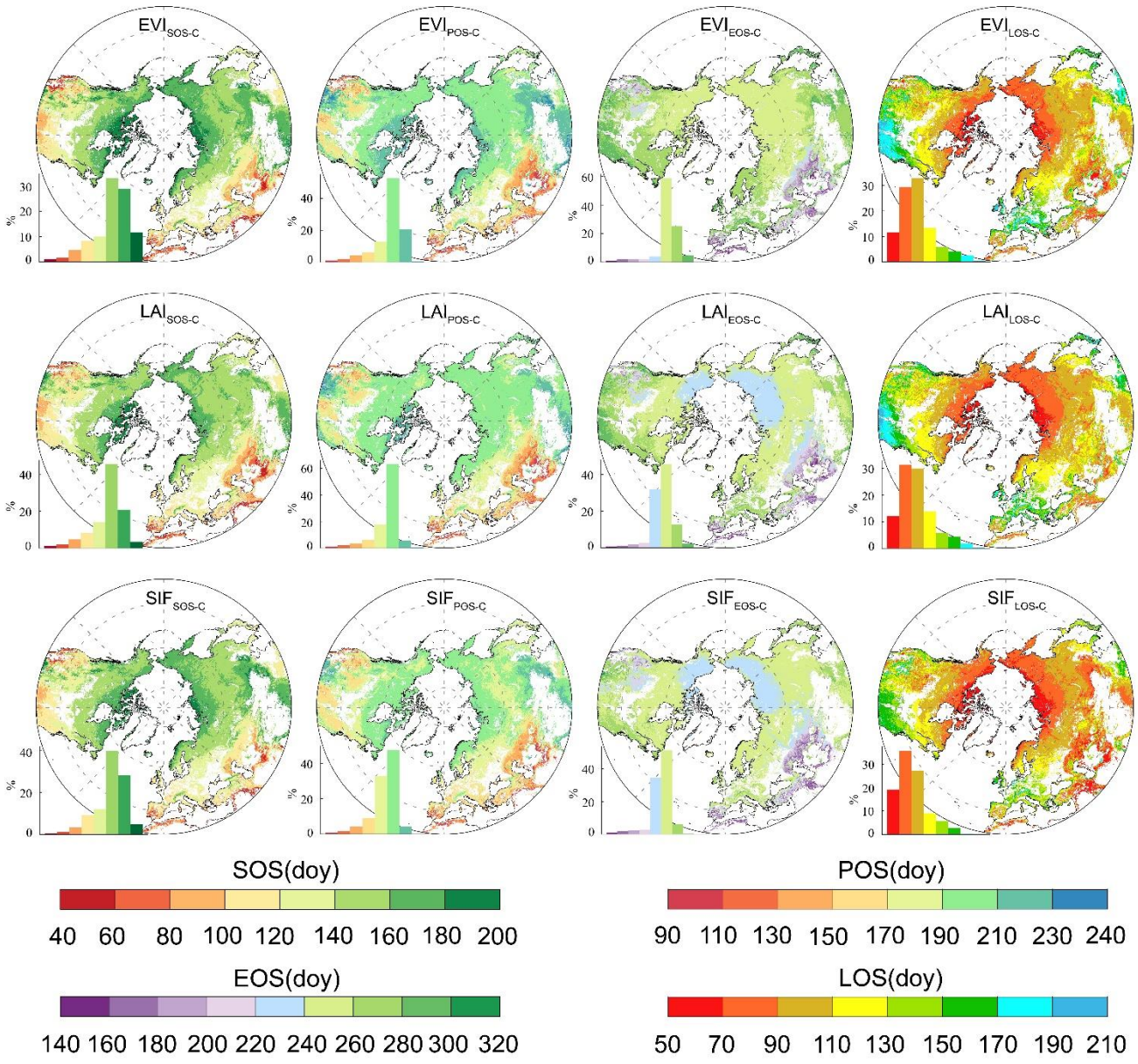


Figure S2: The spatial distribution of multi-year average phenological parameters retrieved by different satellite products based on the algorithm of cubic spline interpolation over the period of 2001-2021. Each histogram in the bottom left corner represents the frequency distribution of the corresponding phenological date.

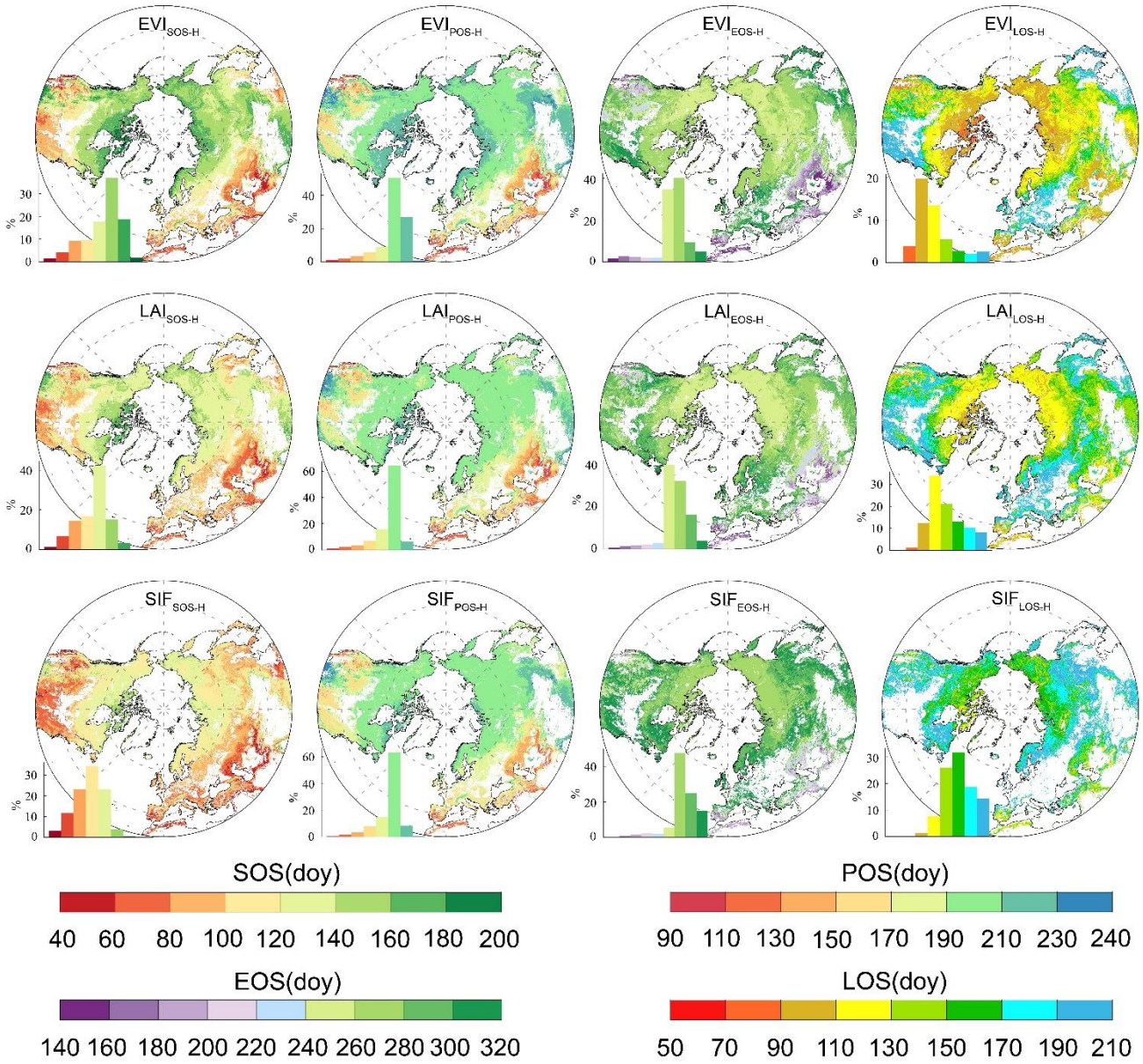


Figure S3: The spatial distribution of multi-year average phenological parameters retrieved by different satellite products based on the algorithm of HANTS over the period of 2001-2021. Each histogram in the bottom left corner represents the frequency distribution of the corresponding phenological date.

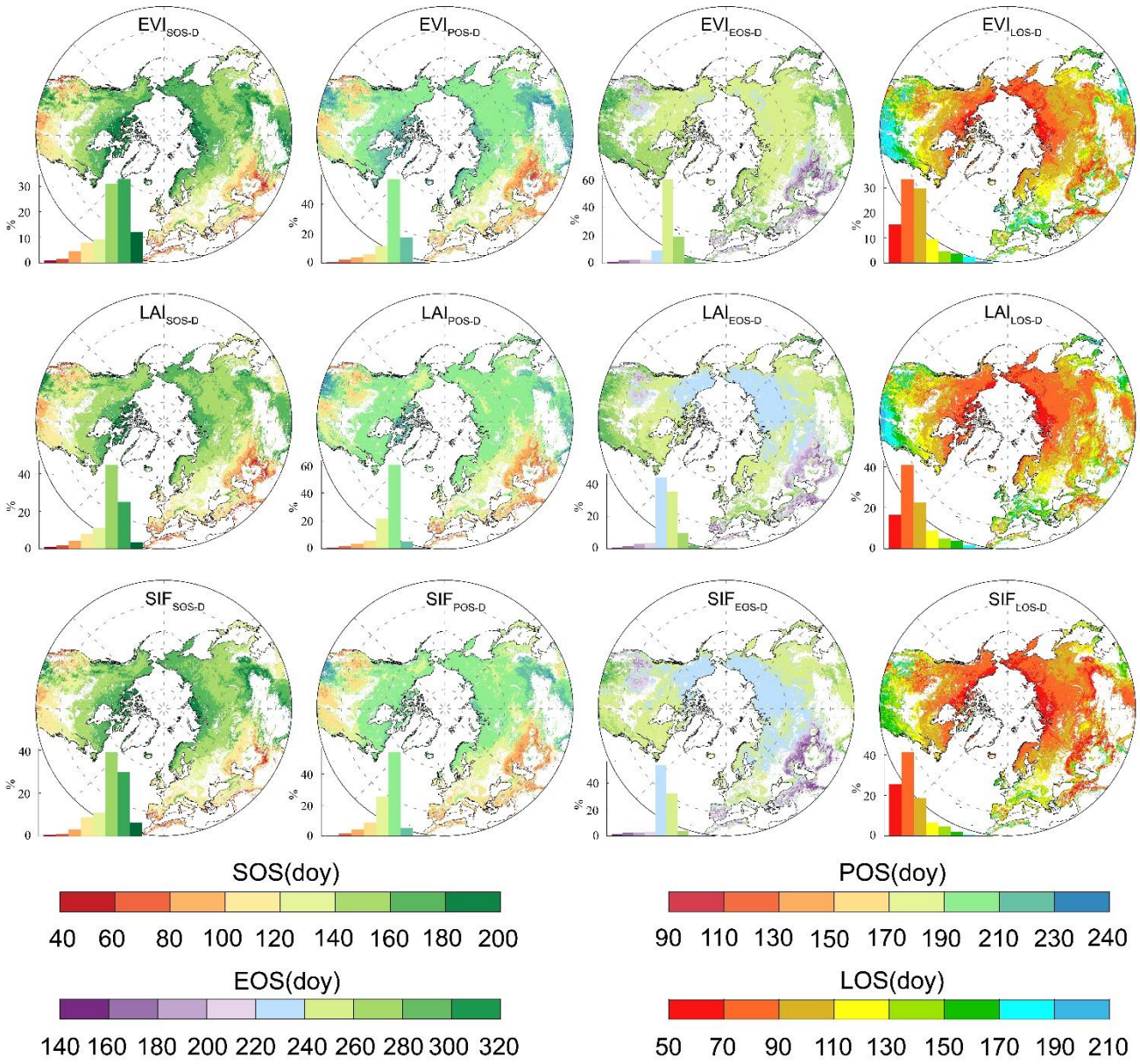


Figure S4: The spatial distribution of multi-year average phenological parameters retrieved by different satellite products based on the algorithm of double logistic over the period of 2001-2021. Each histogram in the bottom left corner represents the frequency distribution of the corresponding phenological date.

Table S3: Average LSP based on different phenological retrieval methods and different satellite products in the mid-high latitudes of the Northern Hemisphere from 2001 to 2021.

Methods	LSP	EVI	LAI	SIF
Cubic spline	SOS(d)	148.06	142.32	146.31
	POS(d)	194.10	189.12	186.91
	EOS(d)	253.87	245.49	241.86
	LOS(d)	105.81	103.17	95.55
HANTS	SOS(d)	149.38	131.30	114.85
	POS(d)	205.00	195.11	196.87

Double logistic	EOS(d)	257.94	253.36	270.47
	LOS(d)	108.56	122.06	155.62
	SOS(d)	151.99	146.48	149.97
	POS(d)	194.11	188.73	187.58
	EOS(d)	249.72	240.60	236.34
	LOS(d)	97.73	94.12	86.38

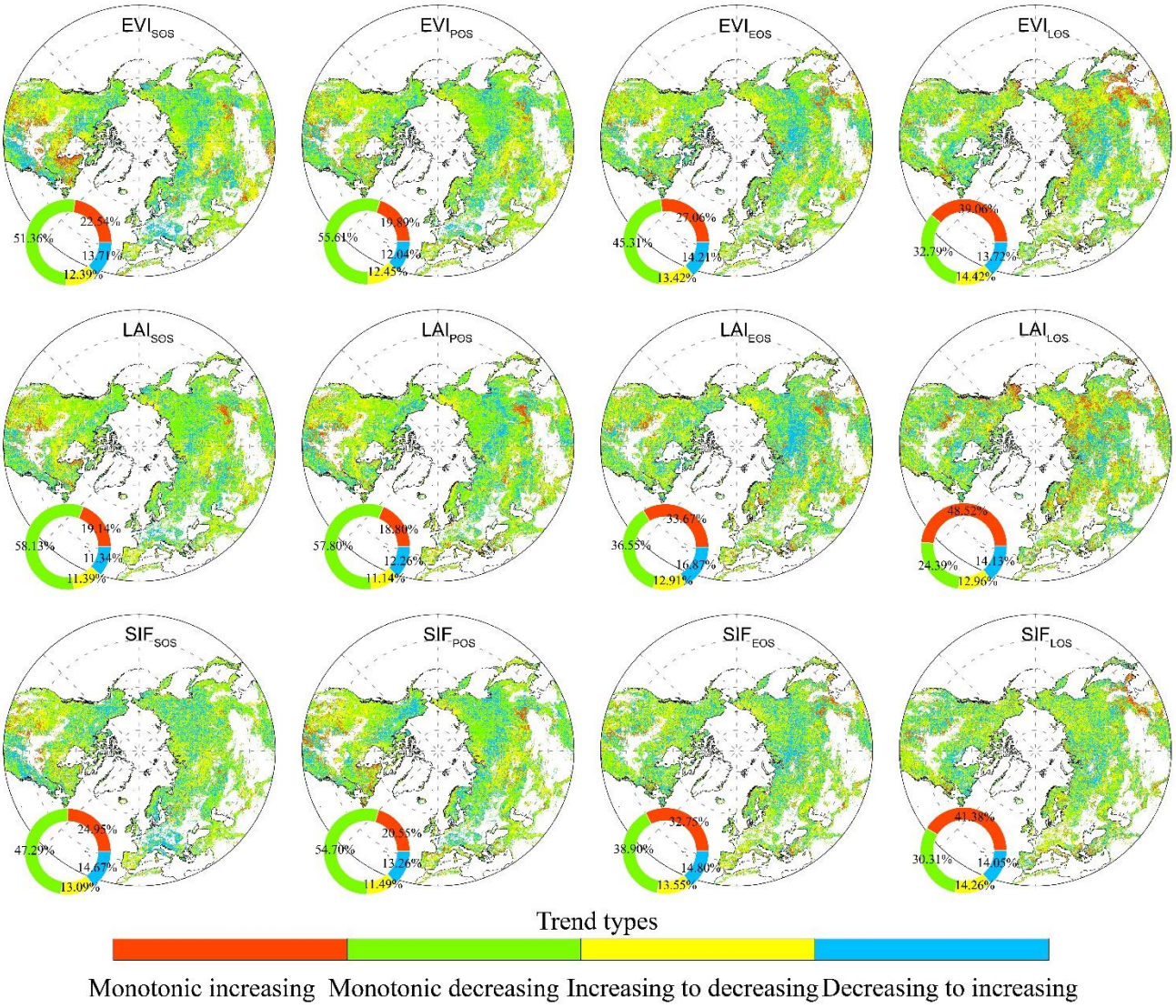


Figure S5: The spatial distribution of average phenological parameter trend types using the EEMD method based on different satellite products and retrieval methods from 2001 to 2021. The pie charts inserted in the bottom left corner of each panel represent the pixel proportions of the 4 different trend types.

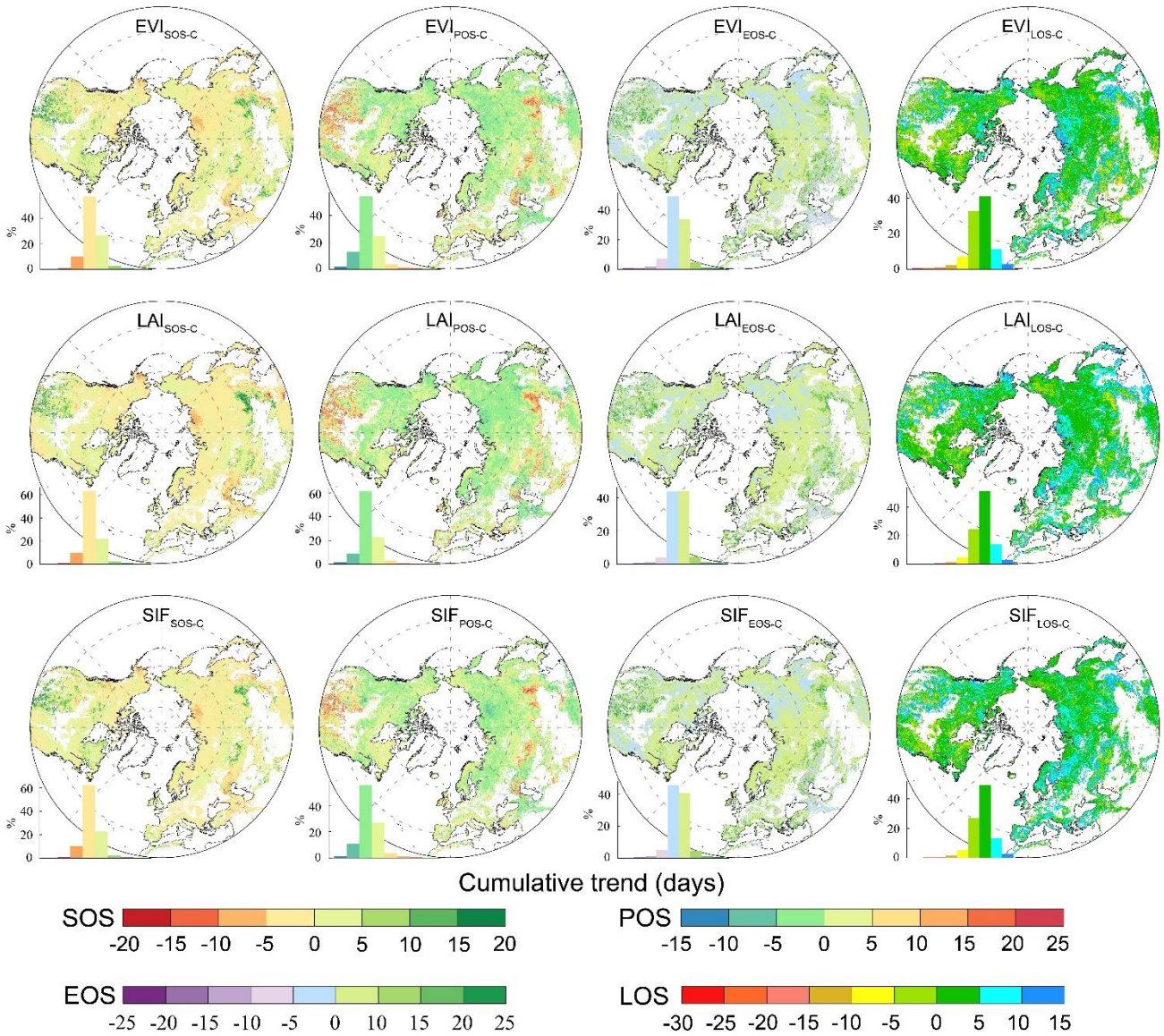


Figure S6: The spatial distribution of the cumulative trend of phenological parameters using the EEMD method based on different satellite products and the algorithm of cubic spline interpolation from 2001 to 2021. The histogram inserted in the bottom left corner of each panel describes the frequency distribution of the corresponding cumulative trend.

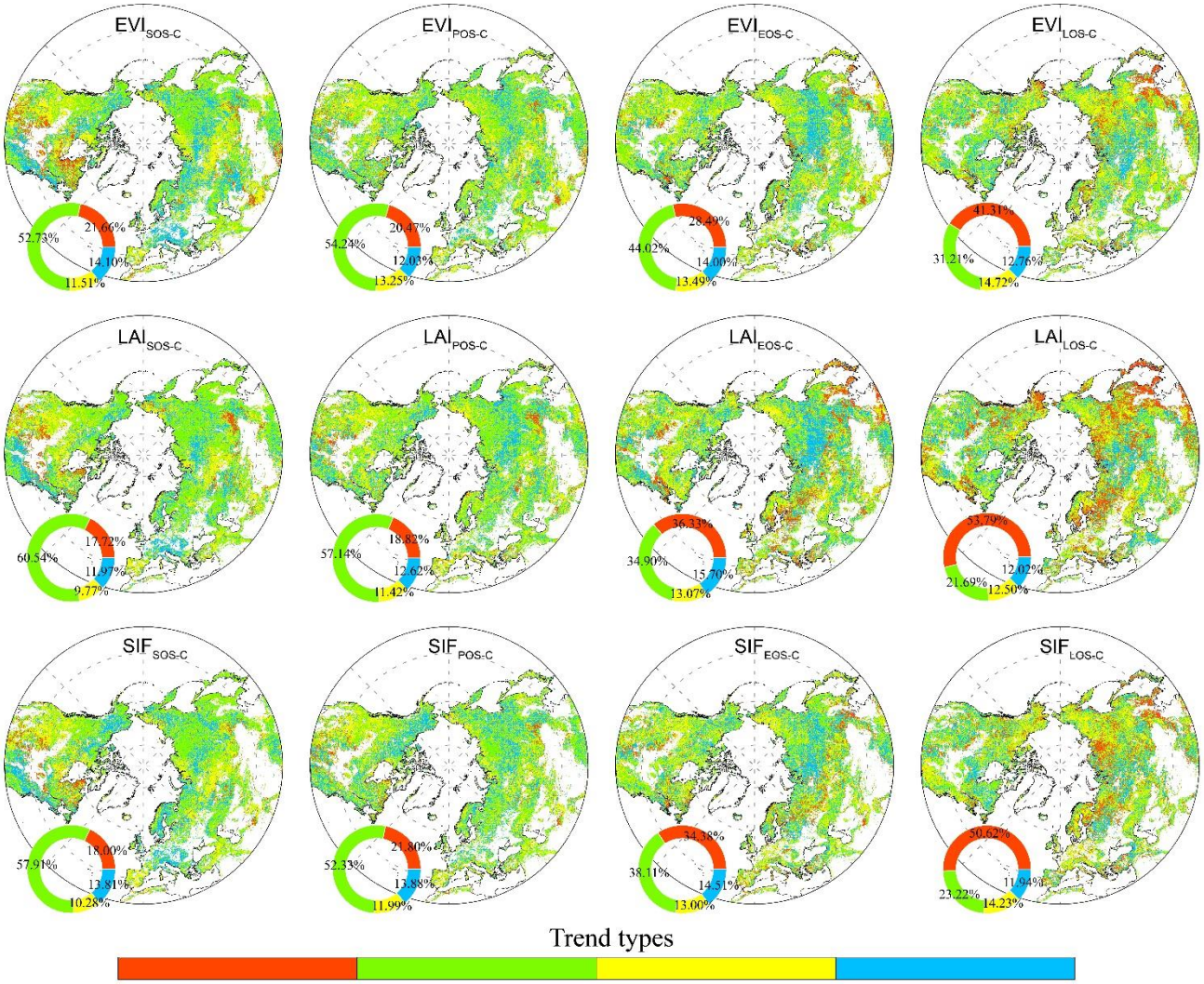


Figure S7: The spatial distribution of phenological parameter trend types using the EEMD method based on different satellite products and the algorithm of cubic spline interpolation from 2001 to 2021. The pie charts inserted in the bottom left corner of each panel represent the pixel proportions of the 4 different trend types.

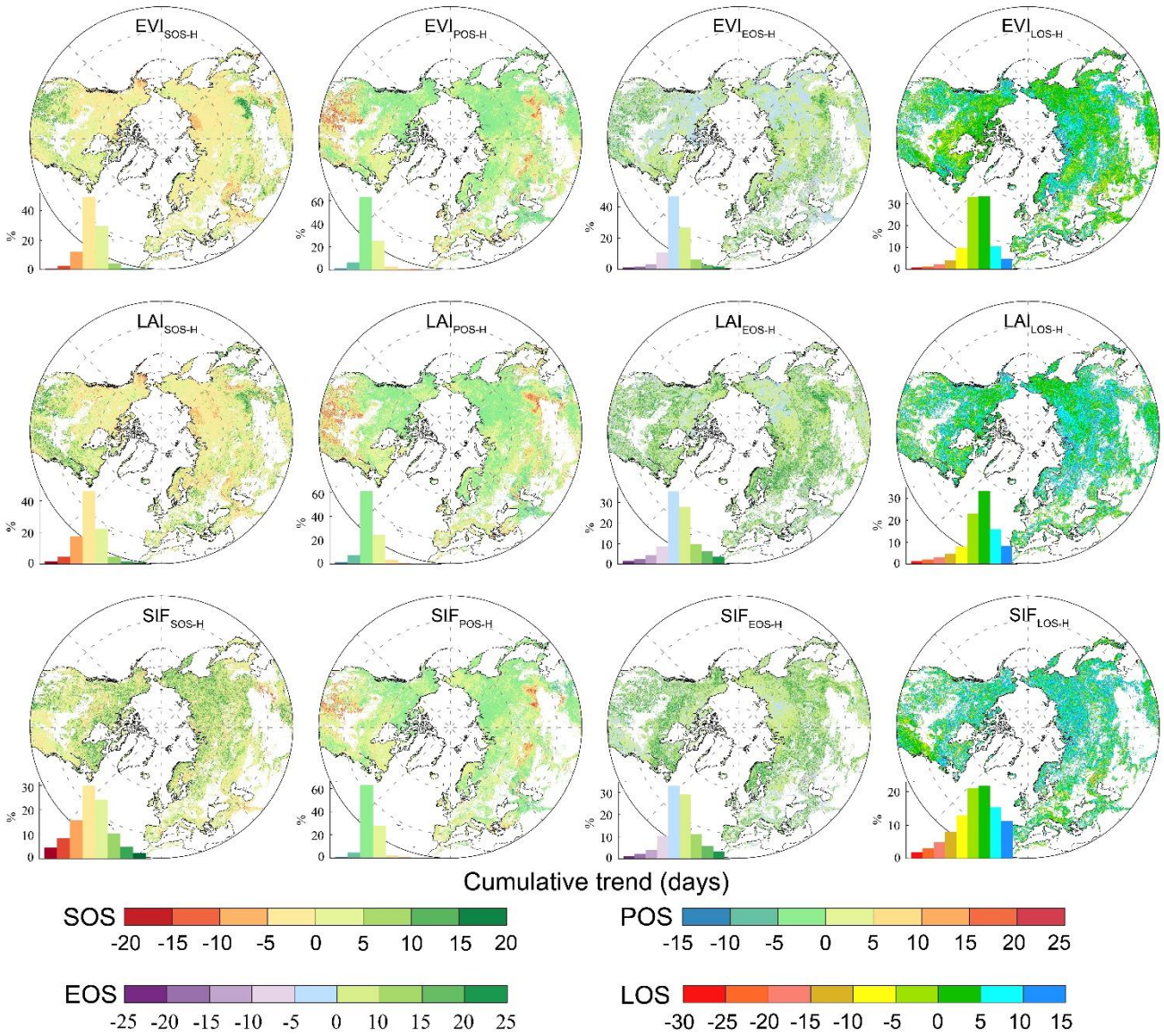


Figure S8: The spatial distribution of the cumulative trend of phenological parameters using the EEMD method based on different satellite products and the algorithm of HANTS from 2001 to 2021. The histogram inserted in the bottom left corner of each panel describes the frequency distribution of the corresponding cumulative trend.

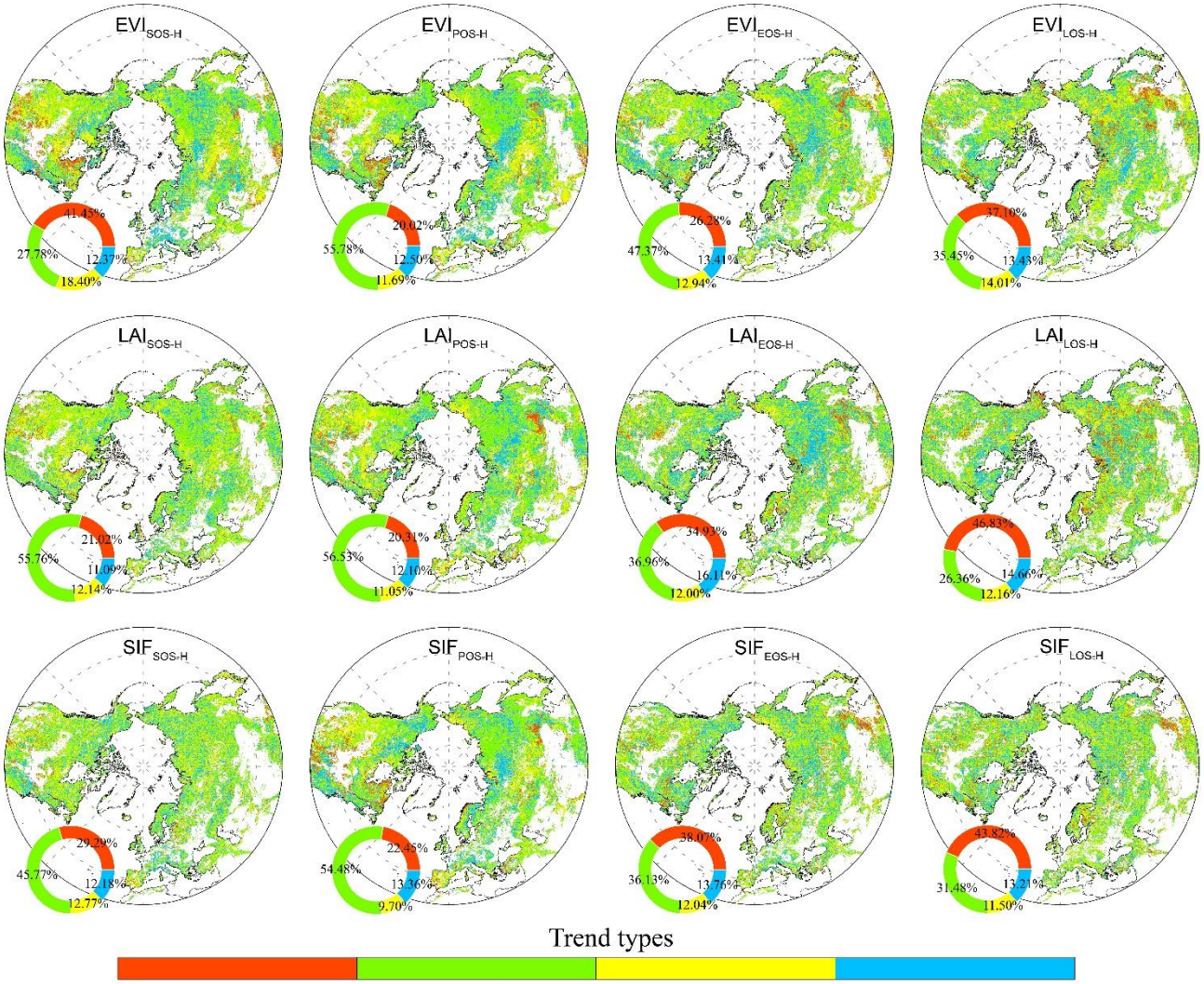


Figure S9: The spatial distribution of phenological parameter trend types using the EEMD method based on different satellite products and the algorithm of HANTS from 2001 to 2021. The pie charts inserted in the bottom left corner of each panel represent the pixel proportions of the 4 different trend types.

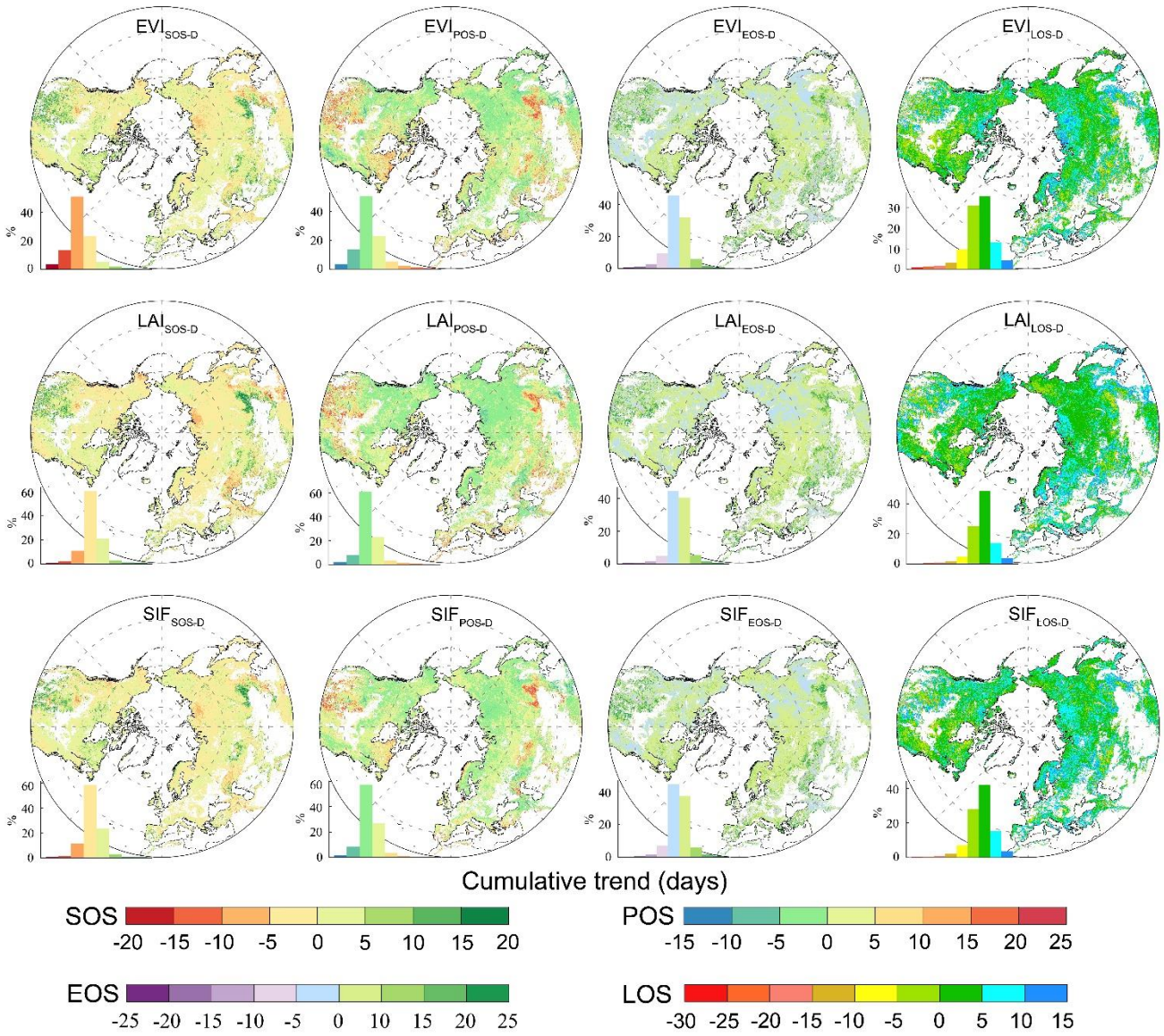


Figure S10: The spatial distribution of the cumulative trend of phenological parameters using the EEMD method based on different satellite products and the algorithm of double logistic from 2001 to 2021. The histogram inserted in the bottom left corner of each panel describes the frequency distribution of the corresponding cumulative trend.

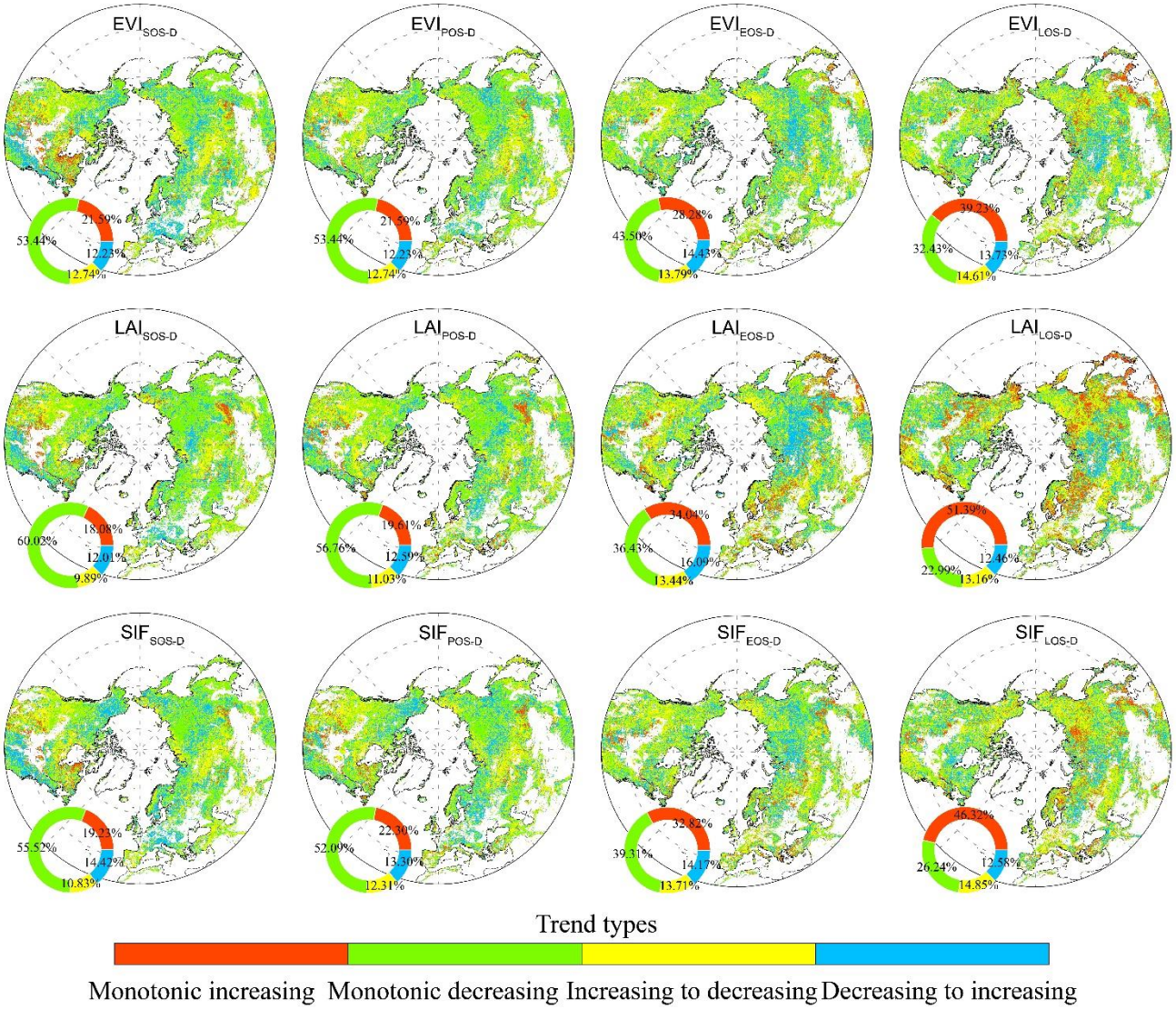


Figure S11: The spatial distribution of phenological parameter trend types using the EEMD method based on different satellite products and the algorithm of double logistic from 2001 to 2021. The pie charts inserted in the bottom left corner of each panel represent the pixel proportions of the 4 different trend types.

Table S4: The average phenological dates and EEMD trends of different vegetation types from 2001 to 2021 in the mid-high latitudes of the Northern Hemisphere.

Vegetation type	EVI（d）± EVI_{std} (d) & trends(d yr^{-1})				LAI（d）± LAI_{std} (d) & trends(d yr^{-1})				SIF（d）± SIF_{std} (d) & trends(d yr^{-1})			
	SOS	POS	EOS	LOS	SOS	POS	EOS	LOS	SOS	POS	EOS	LOS
ENF	145.44 ± 16.08 & -0.02	197.24 ± 10.65 & -0.08	258.41 ± 13.61 & -0.11	112.15 ± 22.89 & -0.13	137.28 ± 12.22 & -0.10	193.67 ± 8.353 & -0.07	258.70 ± 15.64 & 0.05	120.84 ± 23.54 & 0.15	135.38 ± 16.00 & -0.07	188.22 ± 9.68 & -0.06	251.30 ± 13.90 & -0.02	115.27 ± 24.18 & -0.03
EBF	112.96 ± 16.70 & -0.08	177.47 ± 18.84 & -0.11	269.94 ± 27.30 & -0.16	147.35 ± 26.62 & -0.11	106.89 ± 17.49 & -0.11	186.02 ± 23.58 & -0.07	281.03 ± 29.33 & -0.004	165.86 ± 27.13 & 0.12	105.96 ± 12.64 & -0.06	171.76 ± 12.42 & -0.06	261.63 ± 17.66 &-0.05	150.42 ± 18.82 & -0.002
DNF	145.21 ± 6.91 & -0.08	196.19 ± 4.63 & -0.09	255.05 ± 6.57 & -0.07	109.86 ± 11.60 & -0.01	138.23 ± 6.87 & -0.12	191.77 ± 3.94 & -0.09	248.58 ± 8.83 & 0.02	110.37 ± 13.75 & 0.14	138.99 ± 10.45 & -0.03	188.78 ± 4.85 & -0.08	251.62 ± 11.20 & -0.08	112.67 ± 19.80 & -0.05
DBF	120.84 ± 14.61 & -0.07	180.7 ± 14.36 & -0.14	279.74 ± 12.63 & -0.06	158.00 ± 22.49 & 0.02	118.03 ± 15.04 & -0.03	180.74 ± 18.16 & -0.06	265.68 ± 16.54 & -0.07	146.59 ± 24.75 & -0.06	115.86 ± 15.43 & -0.07	174.77 ± 13.35 & -0.05	272.37 ± 12.40 & -0.03	156.05 ± 22.96 & -0.01
MF	139.83 ± 13.61 & -0.03	191.22 ± 11.00 & -0.08	260.84 ± 13.67 & -0.05	120.26 ± 21.96 & -0.03	128.44 ± 12.71 & -0.10	186.33 ± 10.73 & -0.07	258.37 ± 15.00 & 0.05	129.28 ± 22.01 & 0.14	133.42 ± 14.87 & -0.01	183.85 ± 9.82 & -0.06	254.97 ± 14.92 & -0.04	120.95 ± 26.20 & -0.05
CS	159.70 ± 14.12 & -0.14	204.65 ± 12.79 & -0.13	260.34 ± 13.45 & -0.09	101.06 ± 14.18 & -0.01	153.36 ± 13.25 & -0.18	201.50 ± 11.44 & -0.13	255.26 ± 10.79 & -0.08	102.59 ± 15.45 & 0.06	148.15 ± 15.69 & -0.02	198.32 ± 11.49 & -0.12	258.70 ± 11.92. & -0.07	111.10 ± 18.88 & 0.003
OS	167.73 ± 11.29 & -0.01	206.90 ± 7.73 & -0.10	251.26 ± 9.11 & -0.03	83.18 ± 12.21 & 0.11	154.53 ± 9.77 & -0.11	195.99 ± 6.61 & -0.08	242.29 ± 8.61 & -0.01	87.51 ± 11.18 & 0.09	152.12 ± 13.01 & -0.11	199.80 ± 7.66 & -0.06	248.47 ± 9.33 & -0.02	96.13 ± 16.03 & 0.09
WS	144.55 ± 18.85 & 0.01	196.73 ± 13.50 & -0.09	259.20 ± 14.26 & -0.04	112.03 ± 24.63 & -0.02	136.60 ± 16.10 & -0.09	192.19 ± 9.98 & -0.07	254.22 ± 15.76 & -0.002	115.06 ± 24.98 & 0.08	134.00 ± 17.44 & -0.07	188.77 ± 11.14 & -0.07	255.46 ± 14.41 & 0.003	119.53 ± 26.18 & 0.09
SA	149.98 ± 21.22 & -0.09	198.00 ± 16.65 & -0.004	254.34 ± 17.87 & -0.02	101.54 ± 22.66 & 0.04	140.76 ± 18.02 & -0.08	191.23 ± 13.63 & -0.05	248.41 ± 16.63 & 0.002	104.98 ± 22.89 & 0.07	138.05 ± 19.04 & -0.06	190.35 ± 14.31 & -0.02	252.10 ± 16.24 & -0.002	111.84 ± 24.41 & 0.05
GRA	143.59 ± 30.61 & -0.09	189.19 ± 27.49 & -0.07	248.57 ± 29.10 & -0.02	101.75 ± 28.62 & 0.05	135.06 ± 27.61 & -0.09	183.75 ± 23.62 & -0.04	244.83 ± 23.64 & 0.03	106.20 ± 26.95 & 0.12	133.58 ± 25.99 & -0.08	183.92 ± 24.49 & -0.05	246.22 ± 25.97 & 0.01	110.32 ± 28.30 & 0.05

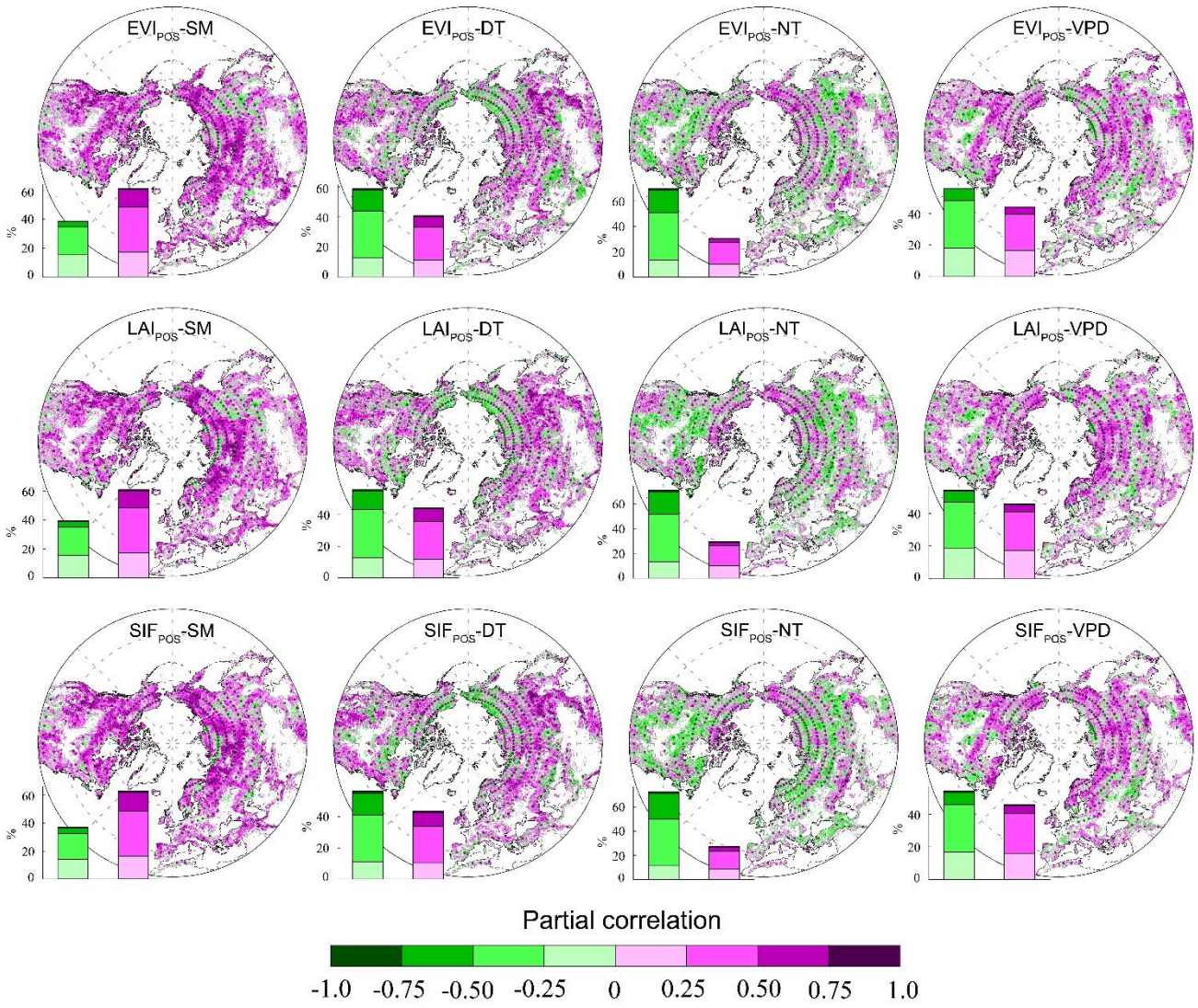


Figure S12: The spatial distribution of the partial correlation coefficients between POS and climate factors (soil moisture (SM), daytime temperature (DT), nighttime temperature (NT), and VPD). The histograms represent the frequency distribution of the corresponding partial correlation coefficients.

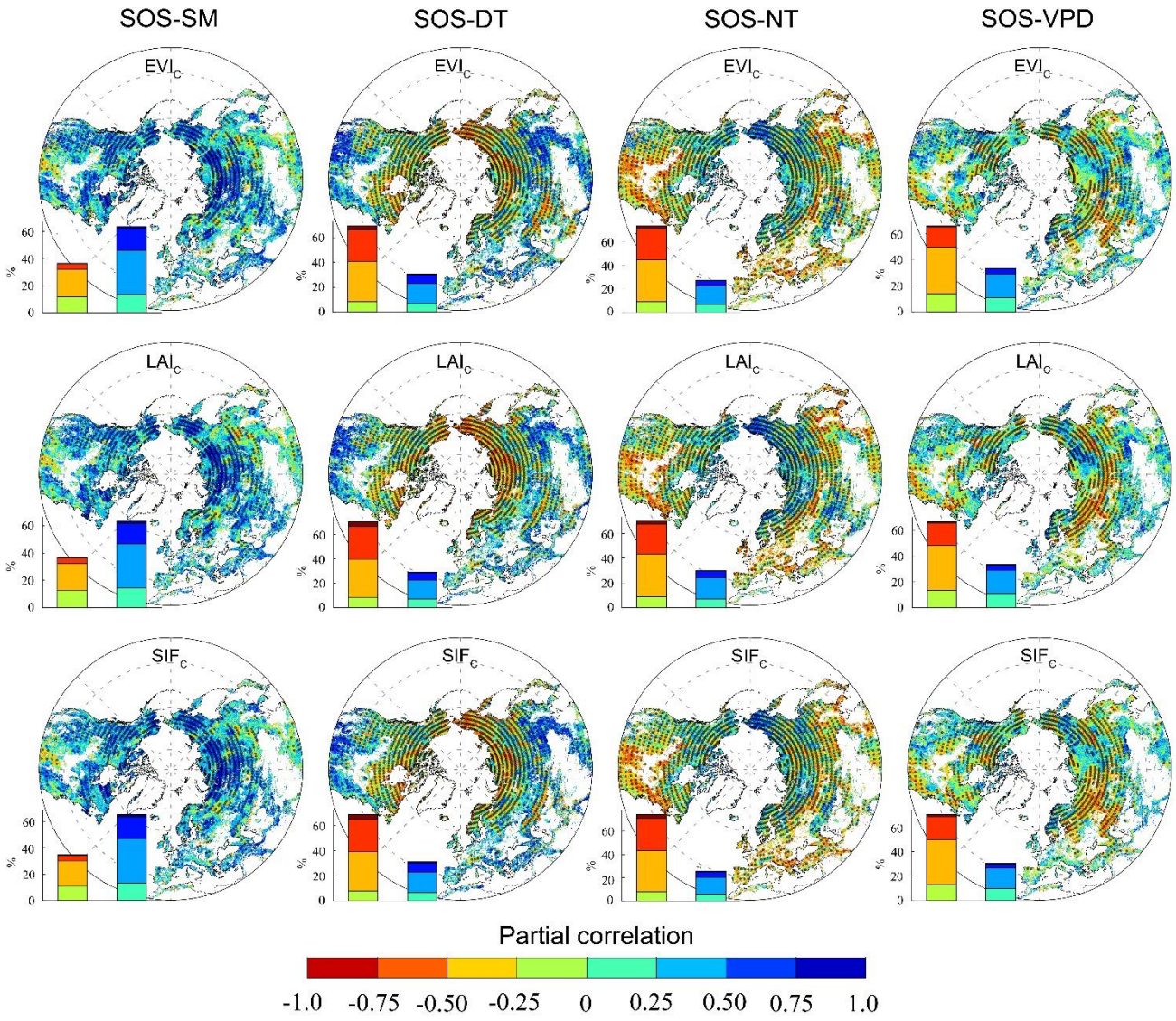


Figure S13: The spatial distribution of the partial correlation coefficients between SOS derived from the algorithm of cubic spline interpolation and climate factors (soil moisture (SM), daytime temperature (DT), nighttime temperature (NT), and VPD). The histograms represent the frequency distribution of the corresponding partial correlation coefficients.

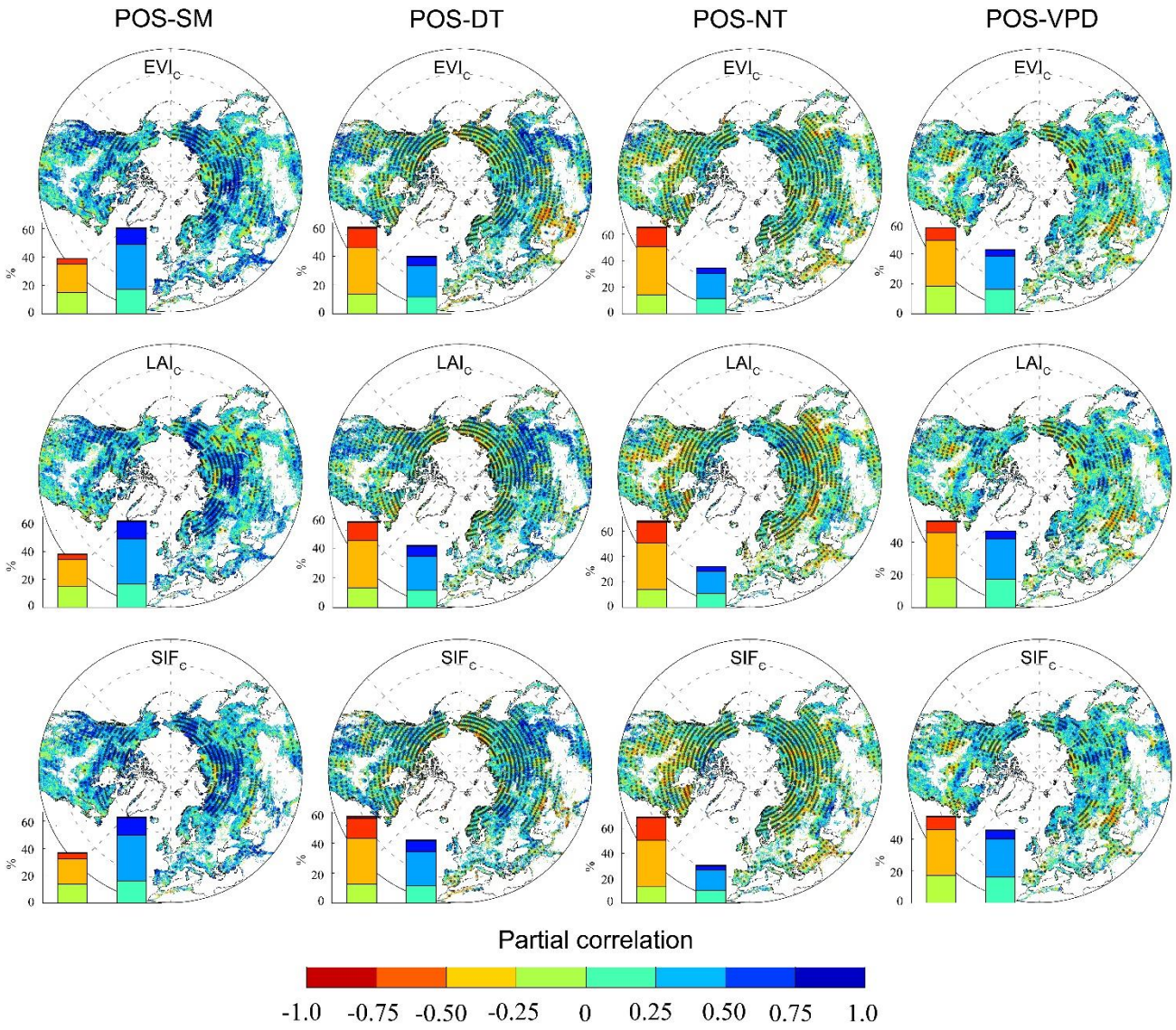


Figure S14: The spatial distribution of the partial correlation coefficients between POS derived from the algorithm of cubic spline interpolation and climate factors (soil moisture (SM), daytime temperature (DT), nighttime temperature (NT), and VPD). The histograms represent the frequency distribution of the corresponding partial correlation coefficients.

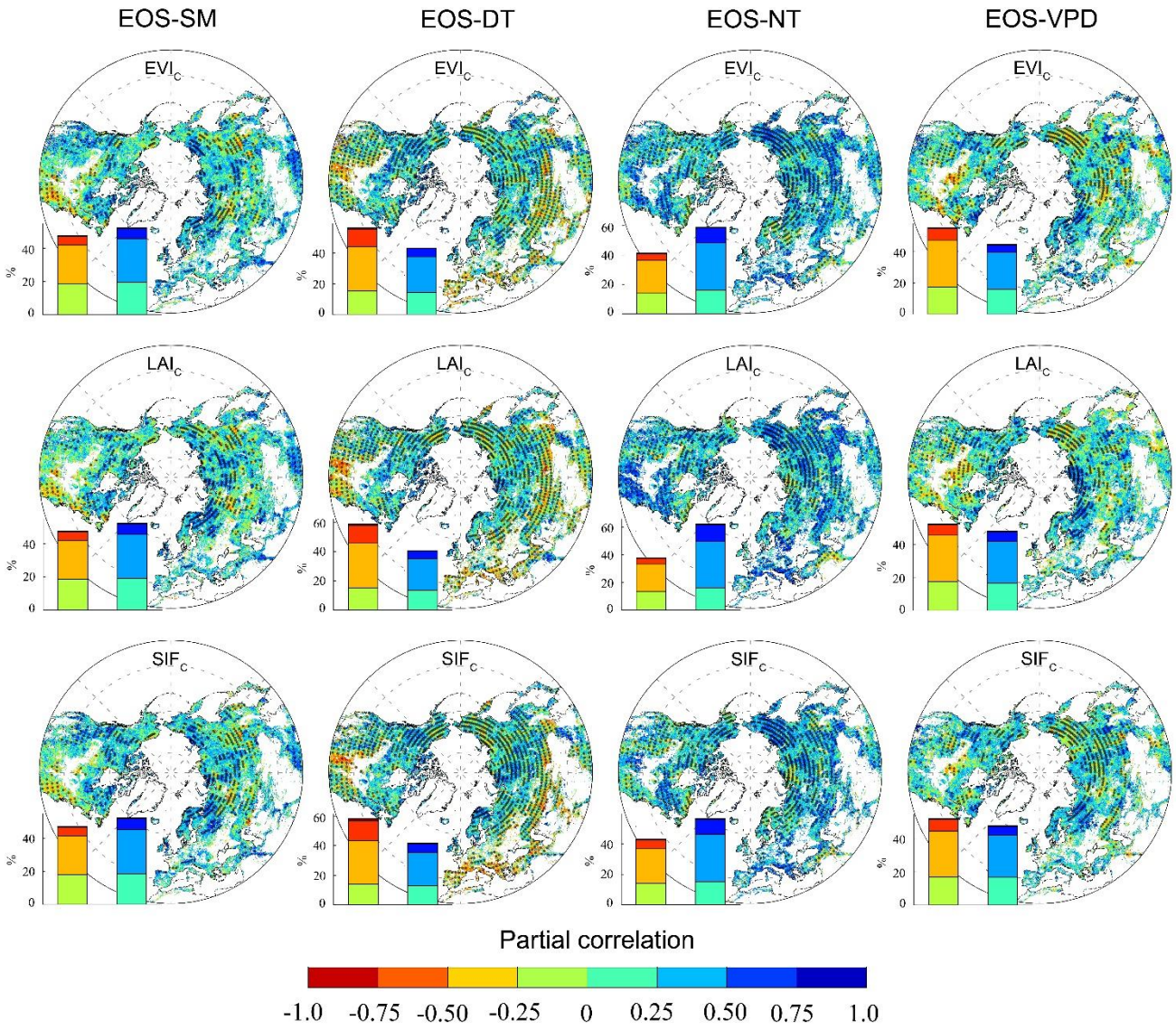


Figure S15: The spatial distribution of the partial correlation coefficients between EOS derived from the algorithm of cubic spline interpolation and climate factors (soil moisture (SM), daytime temperature (DT), nighttime temperature (NT), and VPD). The histograms represent the frequency distribution of the corresponding partial correlation coefficients.

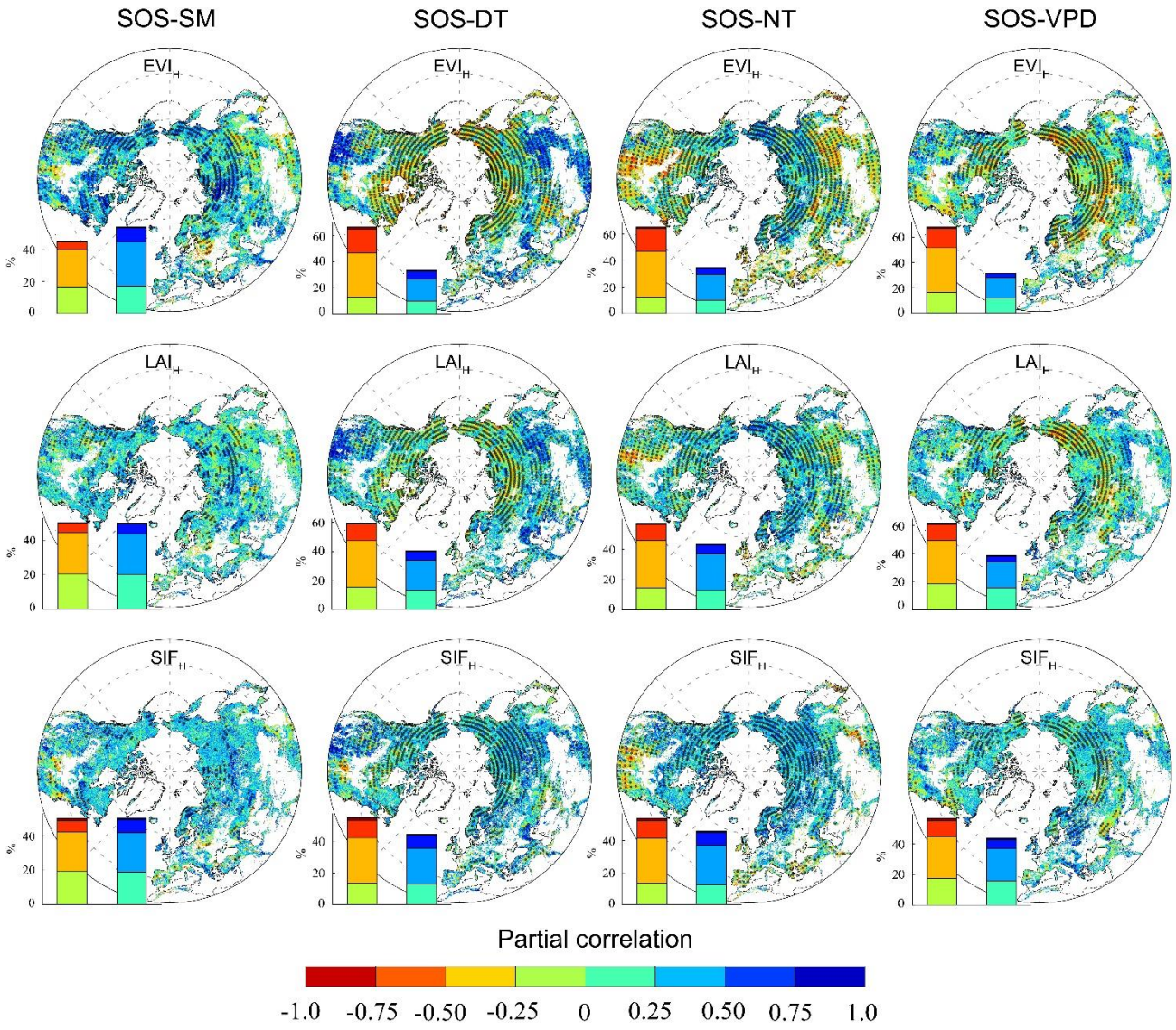


Figure S16: The spatial distribution of the partial correlation coefficients between SOS derived from the algorithm of HANTS and climate factors (soil moisture (SM), daytime temperature (DT), nighttime temperature (NT), and VPD). The histograms represent the frequency distribution of the corresponding partial correlation coefficients.

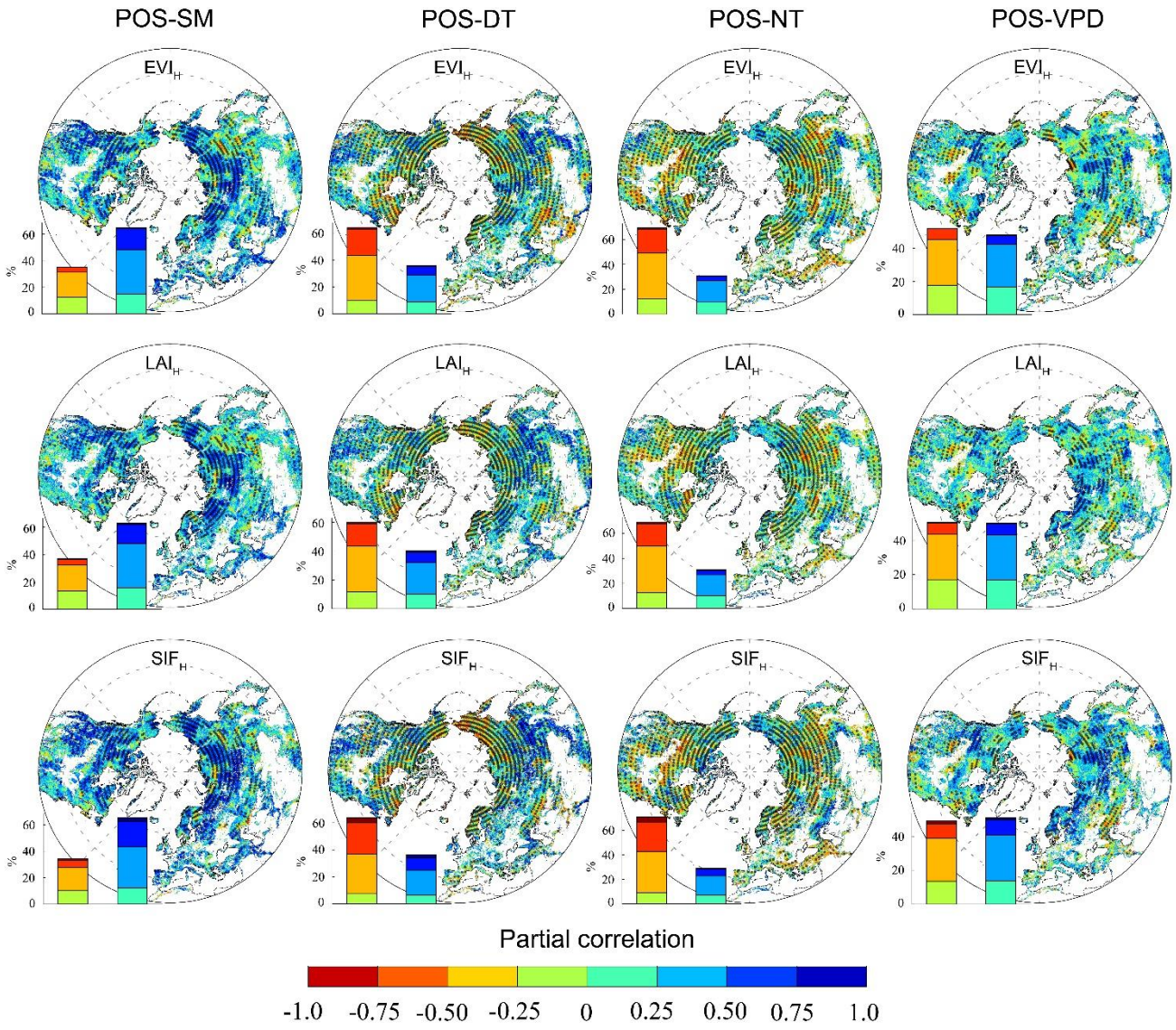


Figure S17: The spatial distribution of the partial correlation coefficients between POS derived from the algorithm of HANTS and climate factors (soil moisture (SM), daytime temperature (DT), nighttime temperature (NT), and VPD). The histograms represent the frequency distribution of the corresponding partial correlation coefficients.

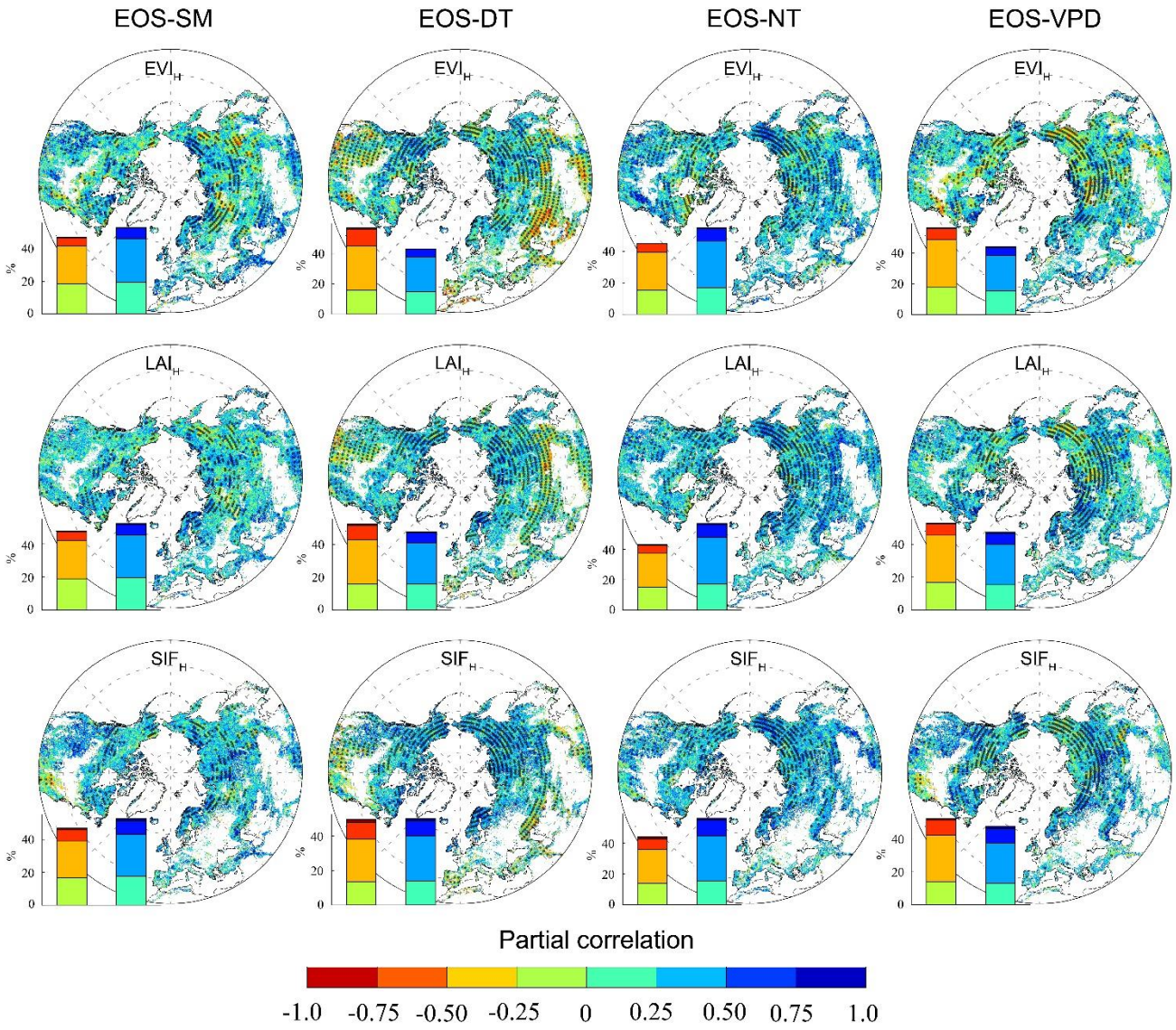


Figure S18: The spatial distribution of the partial correlation coefficients between EOS derived from the algorithm of HANTS and climate factors (soil moisture (SM), daytime temperature (DT), nighttime temperature (NT), and VPD). The histograms represent the frequency distribution of the corresponding partial correlation coefficients.

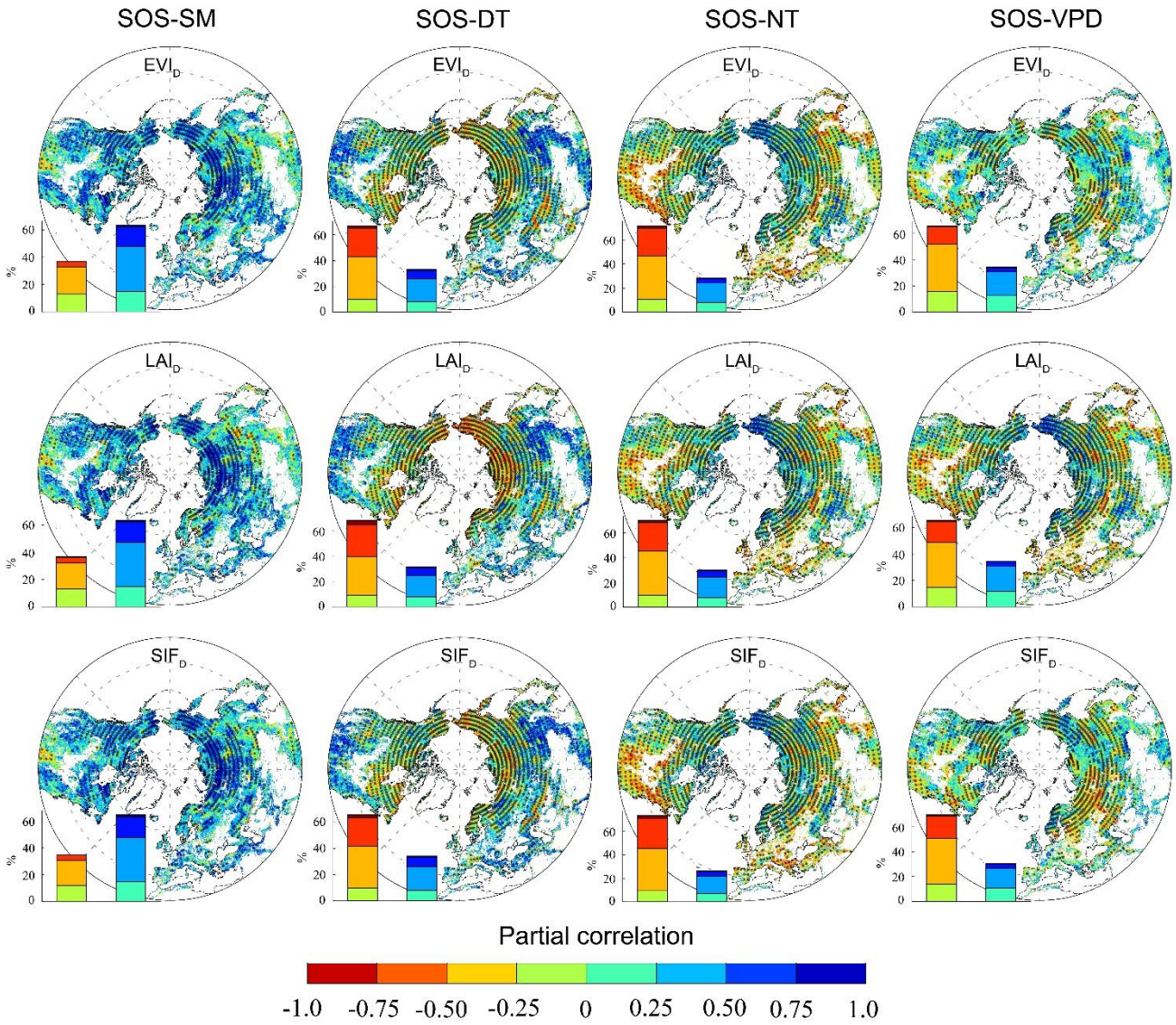


Figure S19: The spatial distribution of the partial correlation coefficients between SOS derived from the algorithm of double logistic and climate factors (soil moisture (SM), daytime temperature (DT), nighttime temperature (NT), and VPD). The histograms represent the frequency distribution of the corresponding partial correlation coefficients.

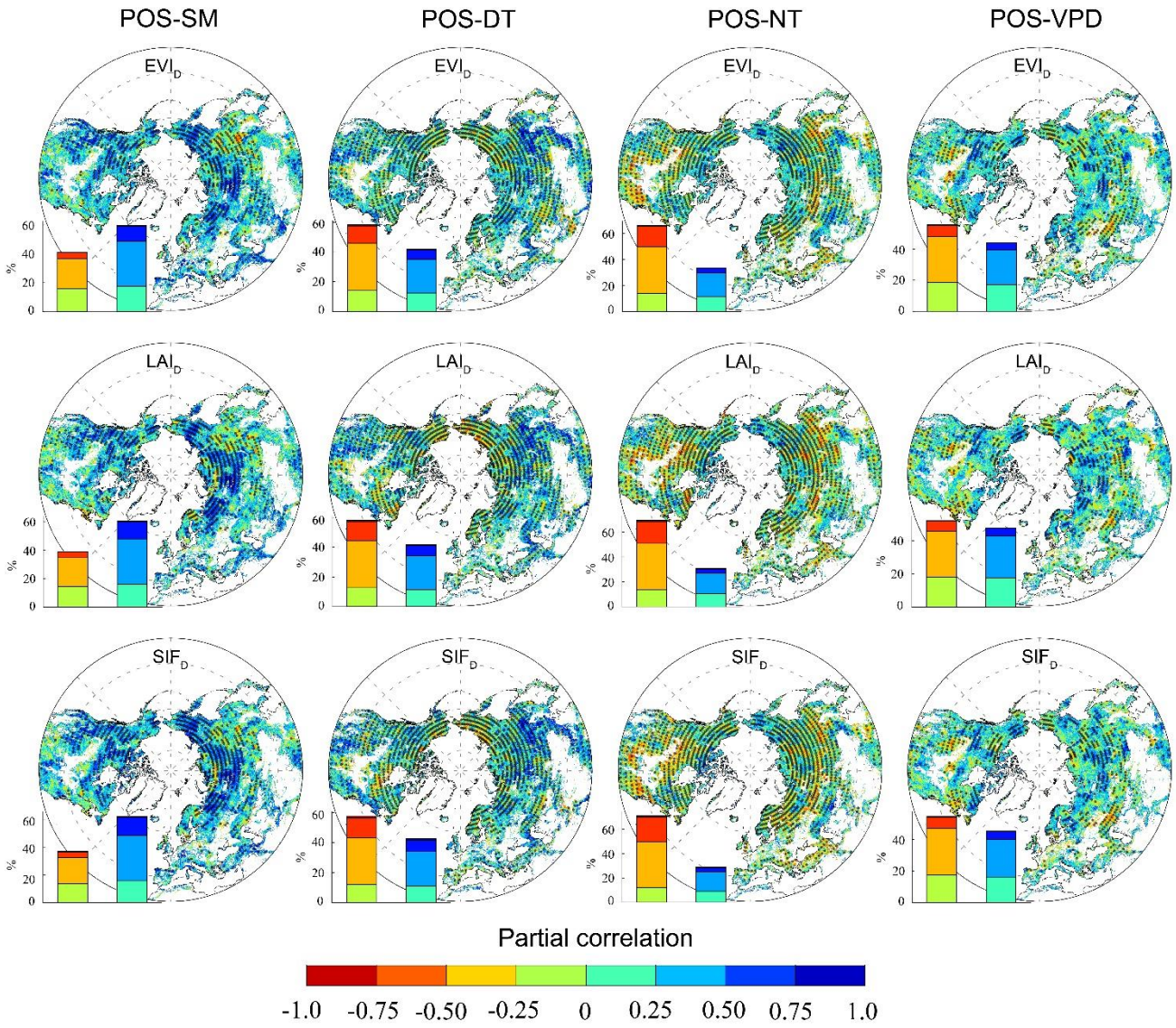


Figure S20: The spatial distribution of the partial correlation coefficients between POS derived from the algorithm of double logistic and climate factors (soil moisture (SM), daytime temperature (DT), nighttime temperature (NT), and VPD). The histograms represent the frequency distribution of the corresponding partial correlation coefficients.

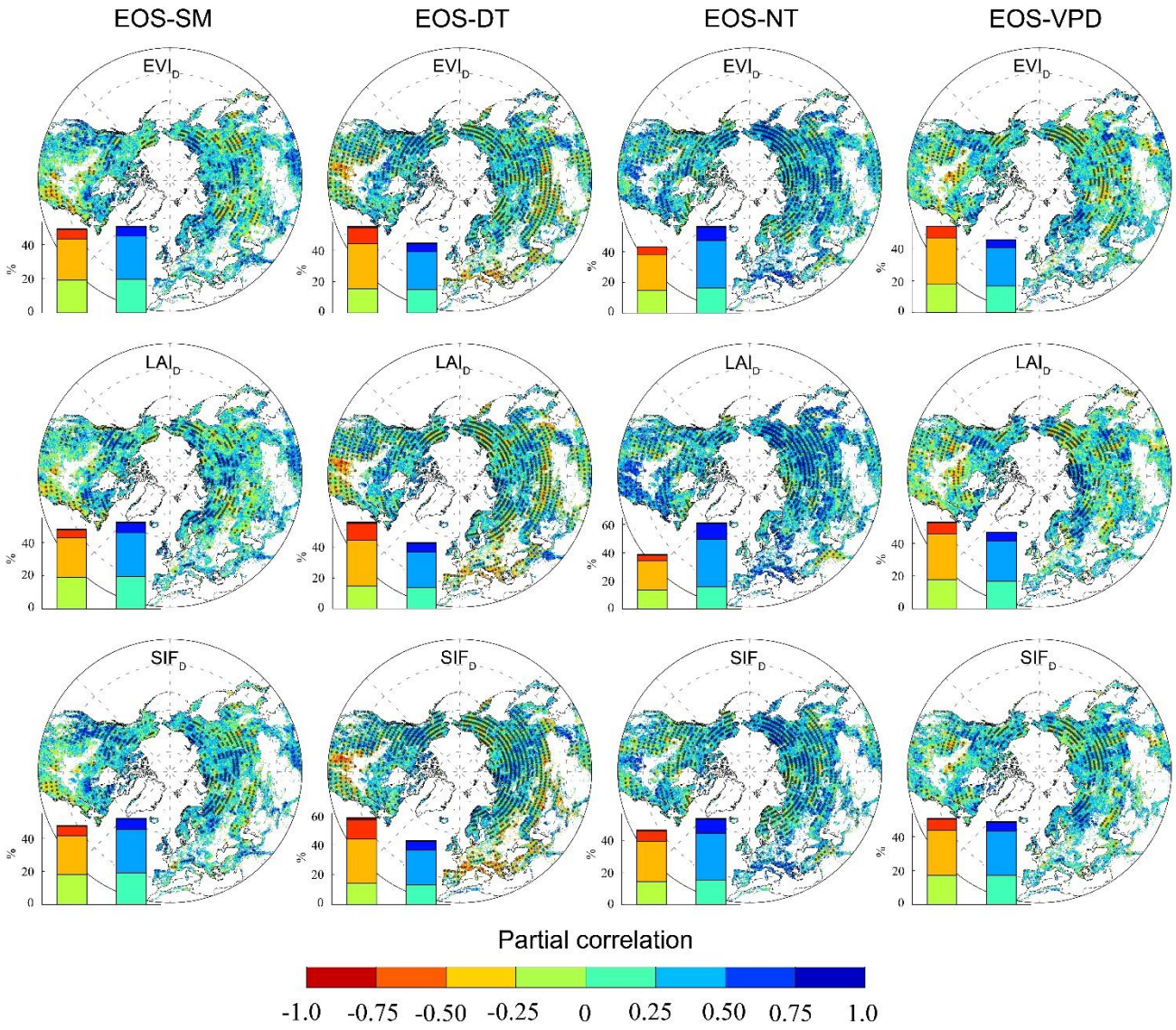


Figure S21: The spatial distribution of the partial correlation coefficients between EOS derived from the algorithm of double logistic and climate factors (soil moisture (SM), daytime temperature (DT), nighttime temperature (NT), and VPD). The histograms represent the frequency distribution of the corresponding partial correlation coefficients.

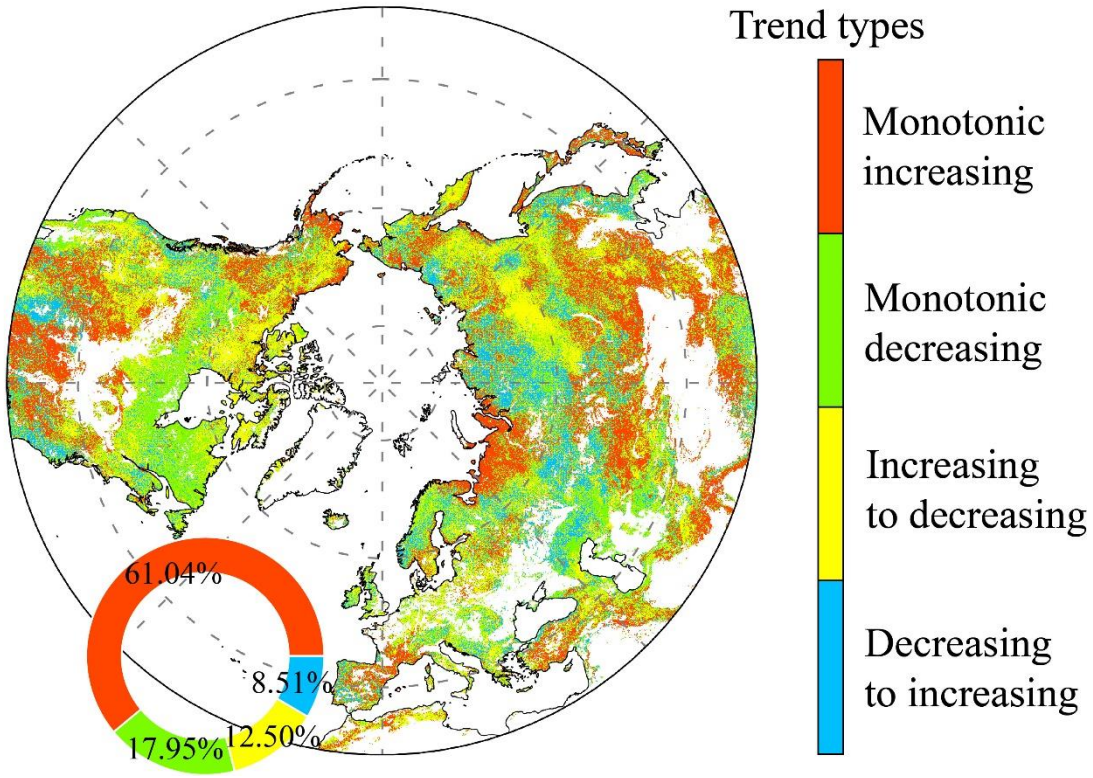


Figure S22: The spatial distribution of NEP trend types based on the regional scale of NEP estimation methods from 2001 to 2021. The pie charts inserted in the bottom left corner of each panel represent the pixel proportions of the 4 different trend types.

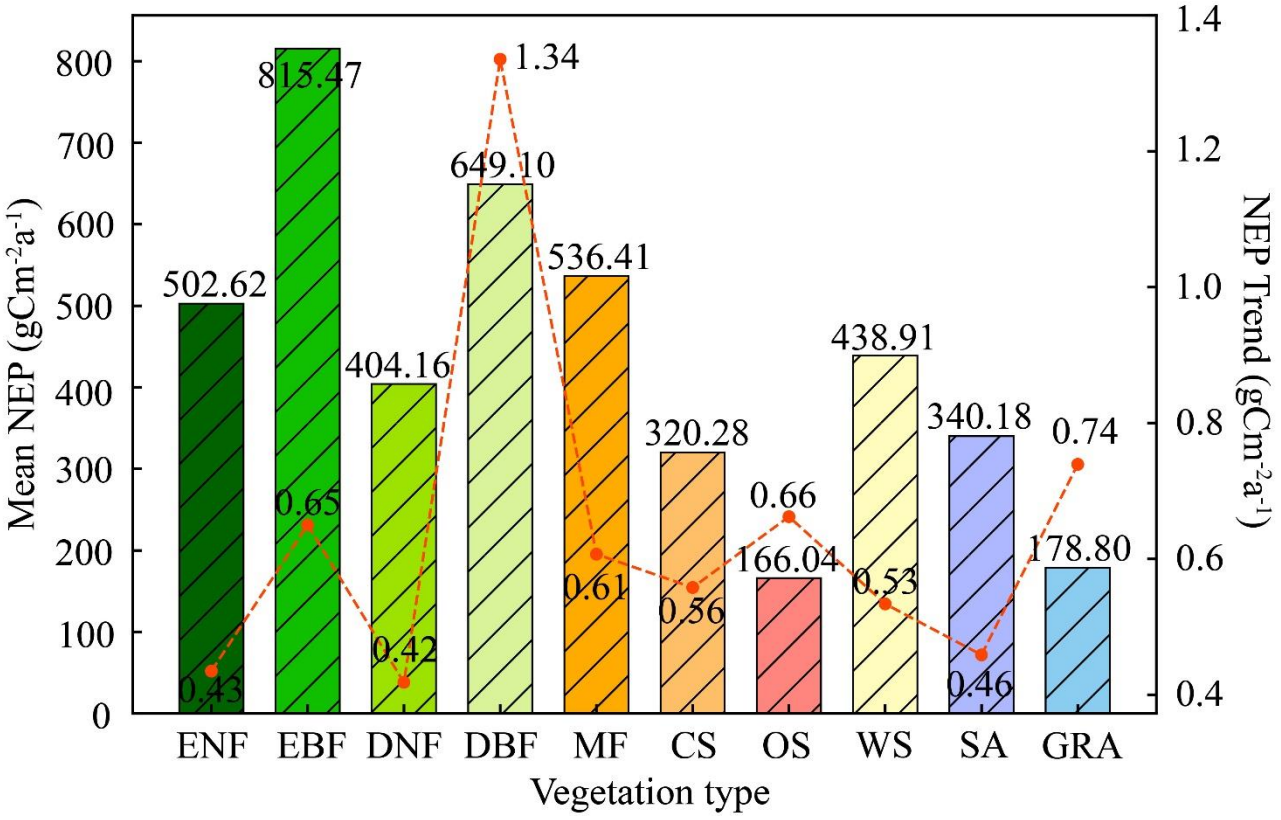


Figure S23: The NEP of different vegetation functional types (histogram) and trend changes (line chart). The left vertical axis represents the multi-year average NEP from 2001 to 2021, while the right vertical axis signifies the trend changes in

NEP based on the EEMD method. ENF: Evergreen Needleleaf Forest; EBF: Evergreen Broadleaf Forests; DNF: Deciduous Needleleaf Forests; DBF: Deciduous Broadleaf Forests; MF: Mixed Forests; CS: Closed Shrublands; OS: Open Shrublands; WS: Woody Savannas; SA: Savannas; GRA: Grasslands;

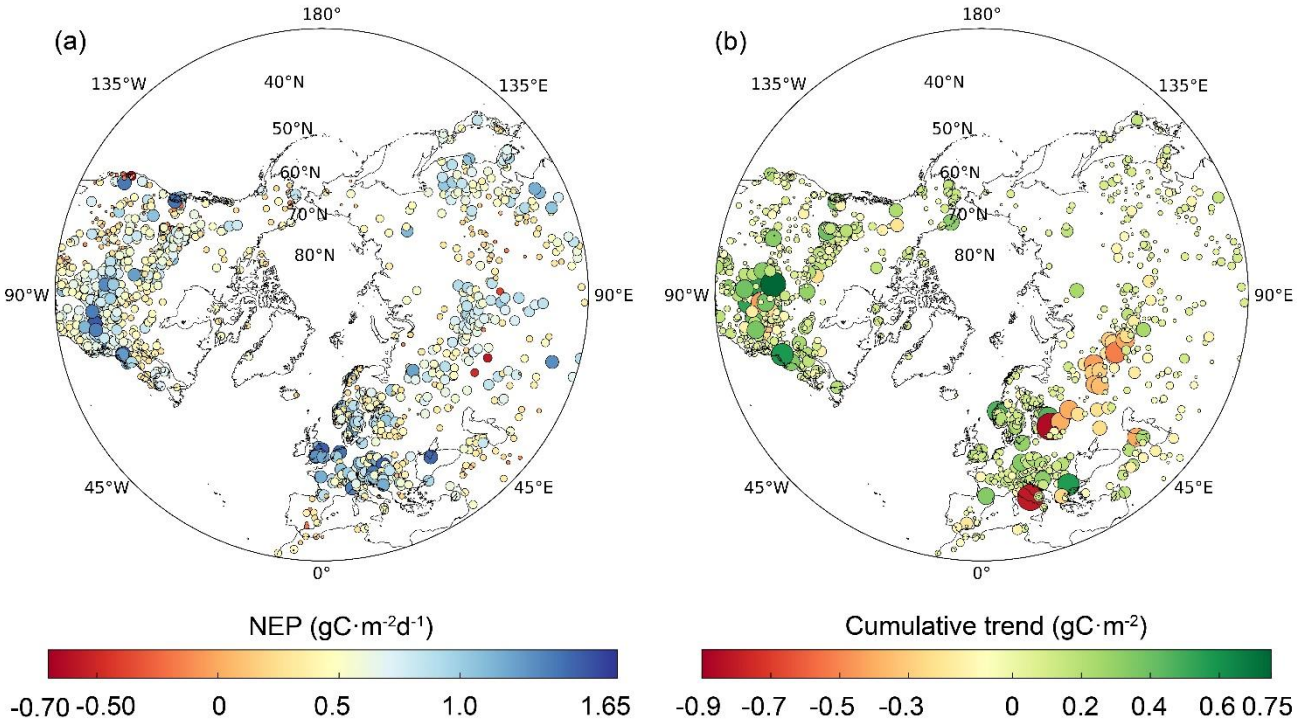


Figure S24: Spatial distribution of multi-year average NEP (a) and cumulative trend changes (b) based on sites from 2001 to 2019.

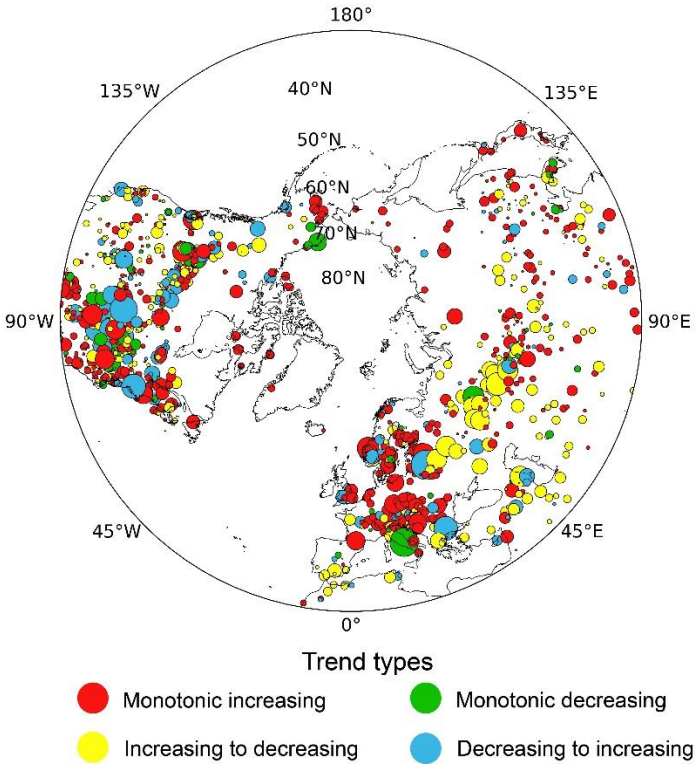


Figure S25: Spatial distribution of NEP trend types based on sites from 2001 to 2019.

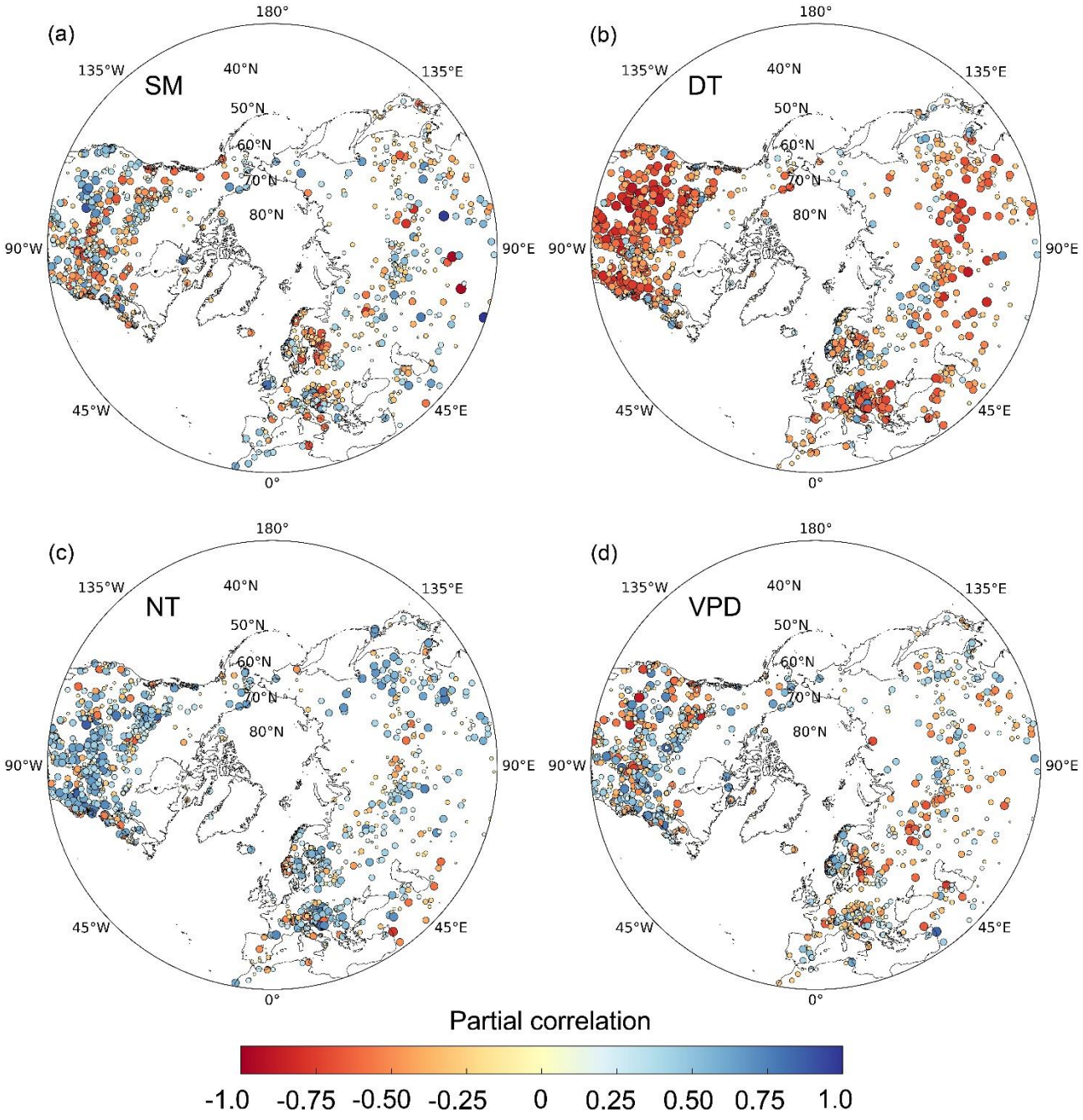


Figure S26: Spatial distribution of partial correlation coefficients between NEP derived from sites and annual average climate factors (soil moisture (SM), daytime temperature (DT), nighttime temperature (NT), and VPD)

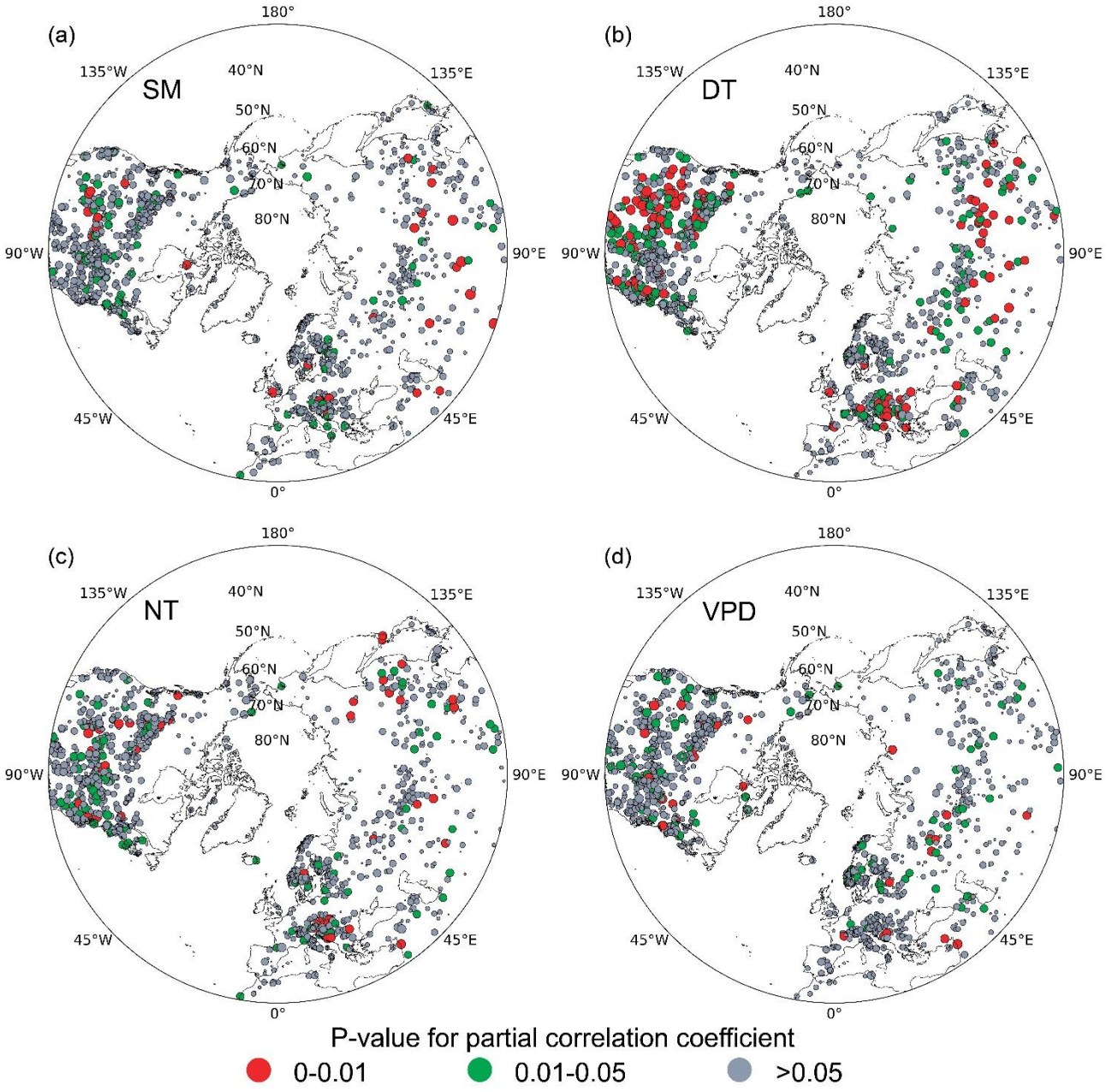


Figure S27: Spatial distribution of p-values for the partial correlation coefficients between NEP derived from sites and annual average climate factors (soil moisture (SM), daytime temperature (DT), nighttime temperature (NT), and VPD). The red, green, and gray points respectively indicate $p < 0.01$, $0.01 \leq p < 0.05$, and $p > 0.05$.

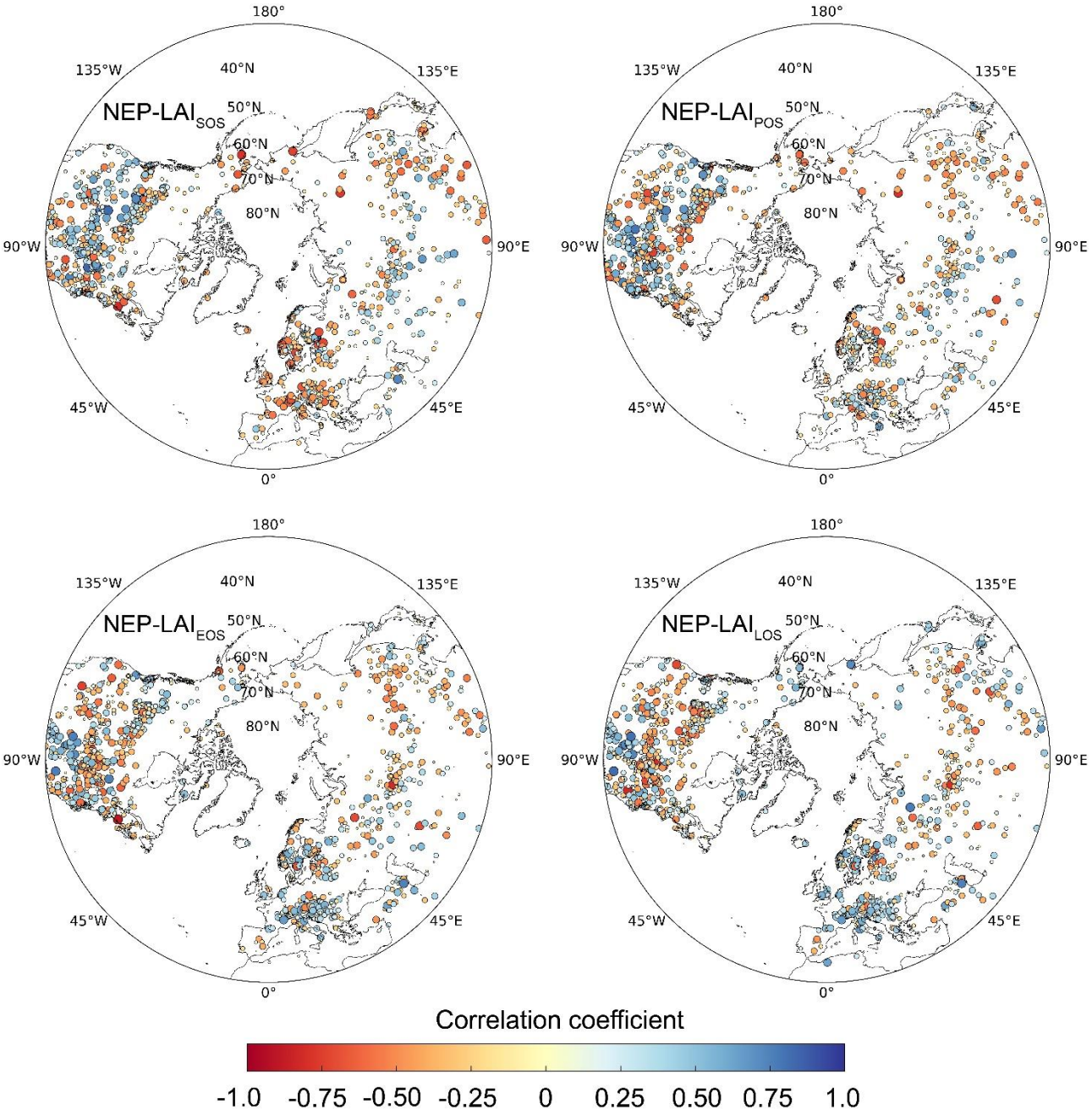


Figure S28: The spatial distribution of the correlation coefficients between vegetation phenological parameters (SOS, POS, EOS and LOS) derived from 500m LAI and NEP at the site scale.

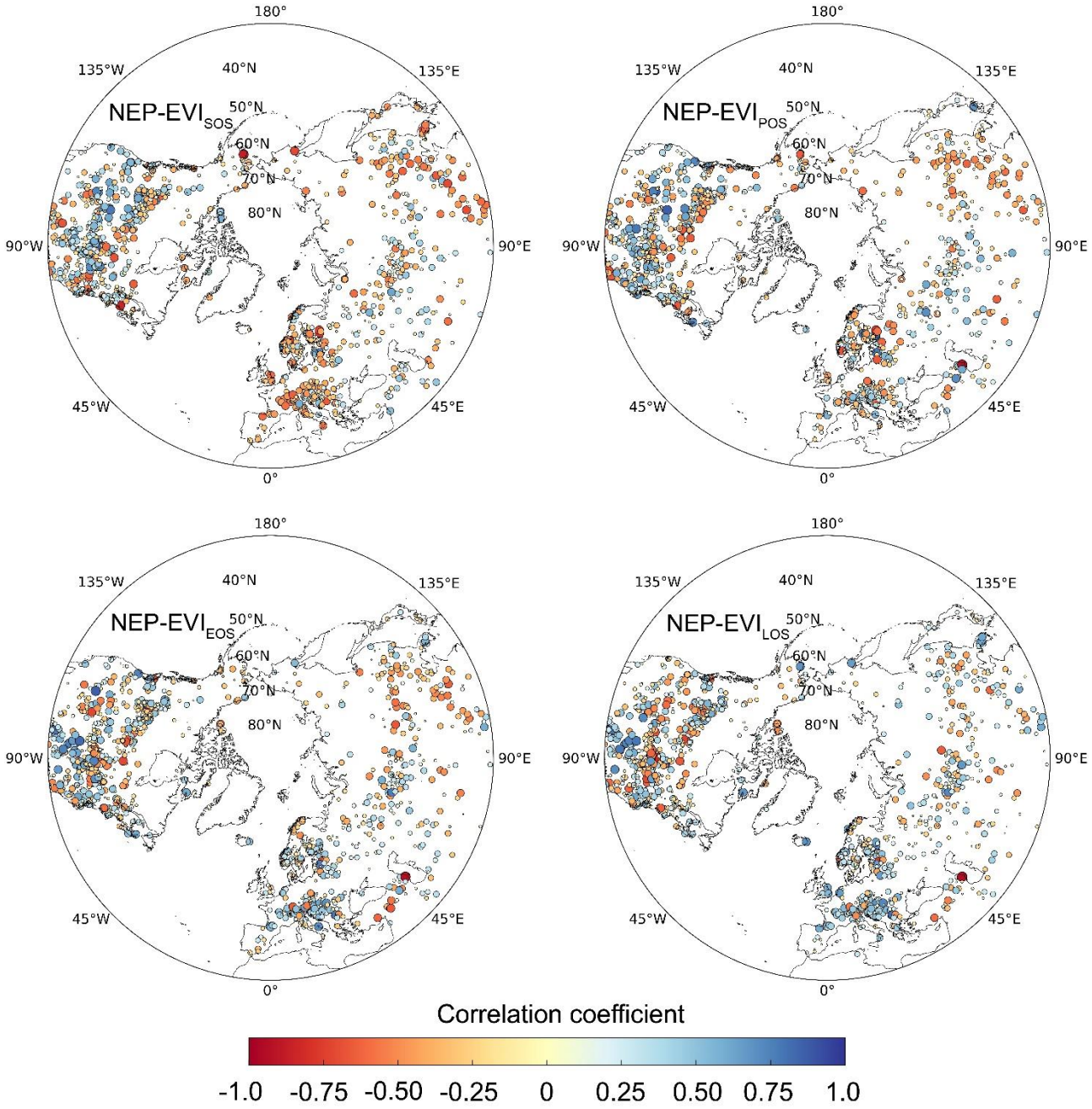


Figure S29: The spatial distribution of the correlation coefficients between vegetation phenological parameters (SOS, POS, EOS and LOS) derived from 500m EVI and NEP at the site scale.

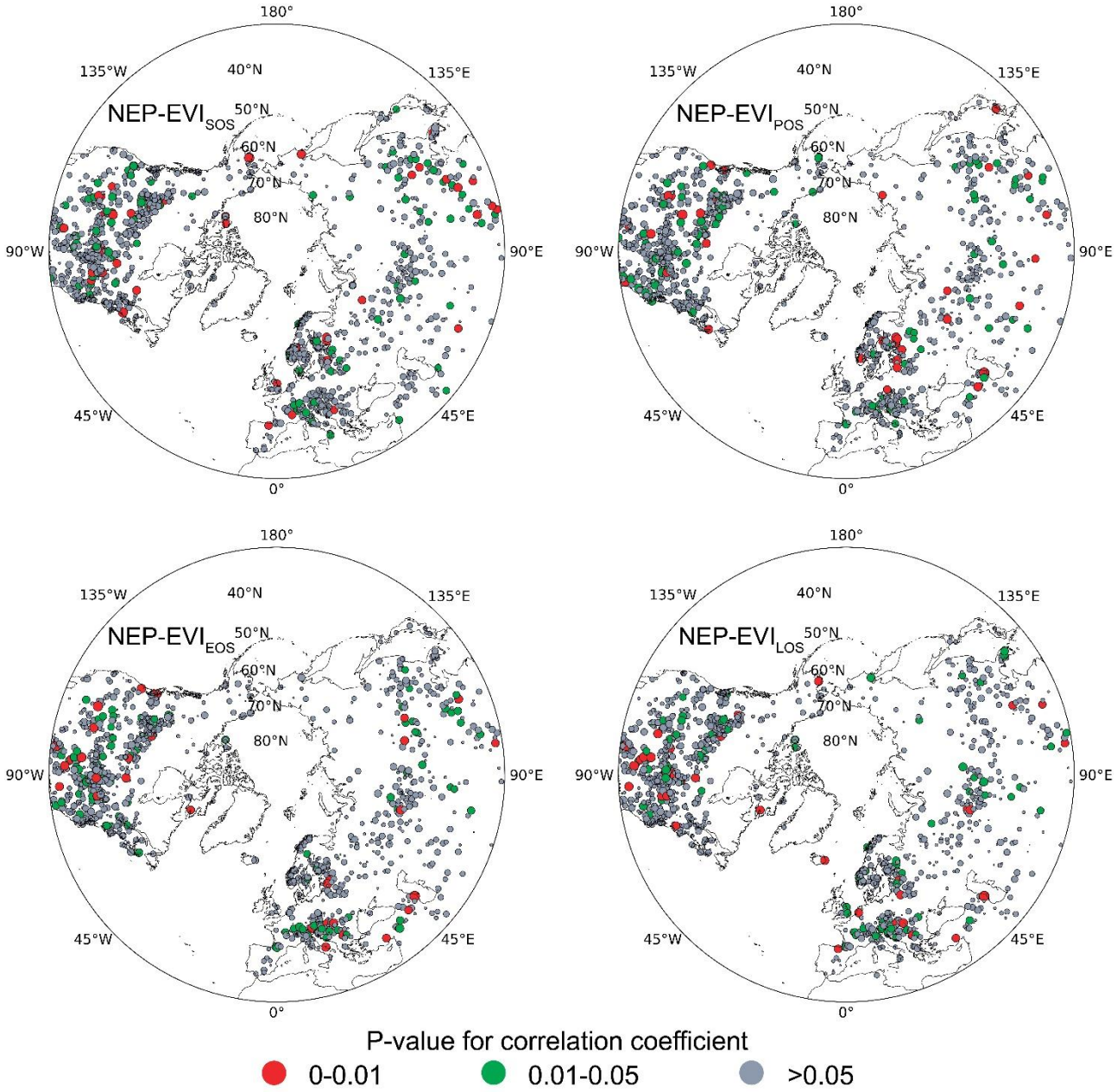


Figure S30: Spatial distribution of p-values for the correlation coefficients between vegetation phenological parameters derived from 500m EVI and NEP at the site scale.

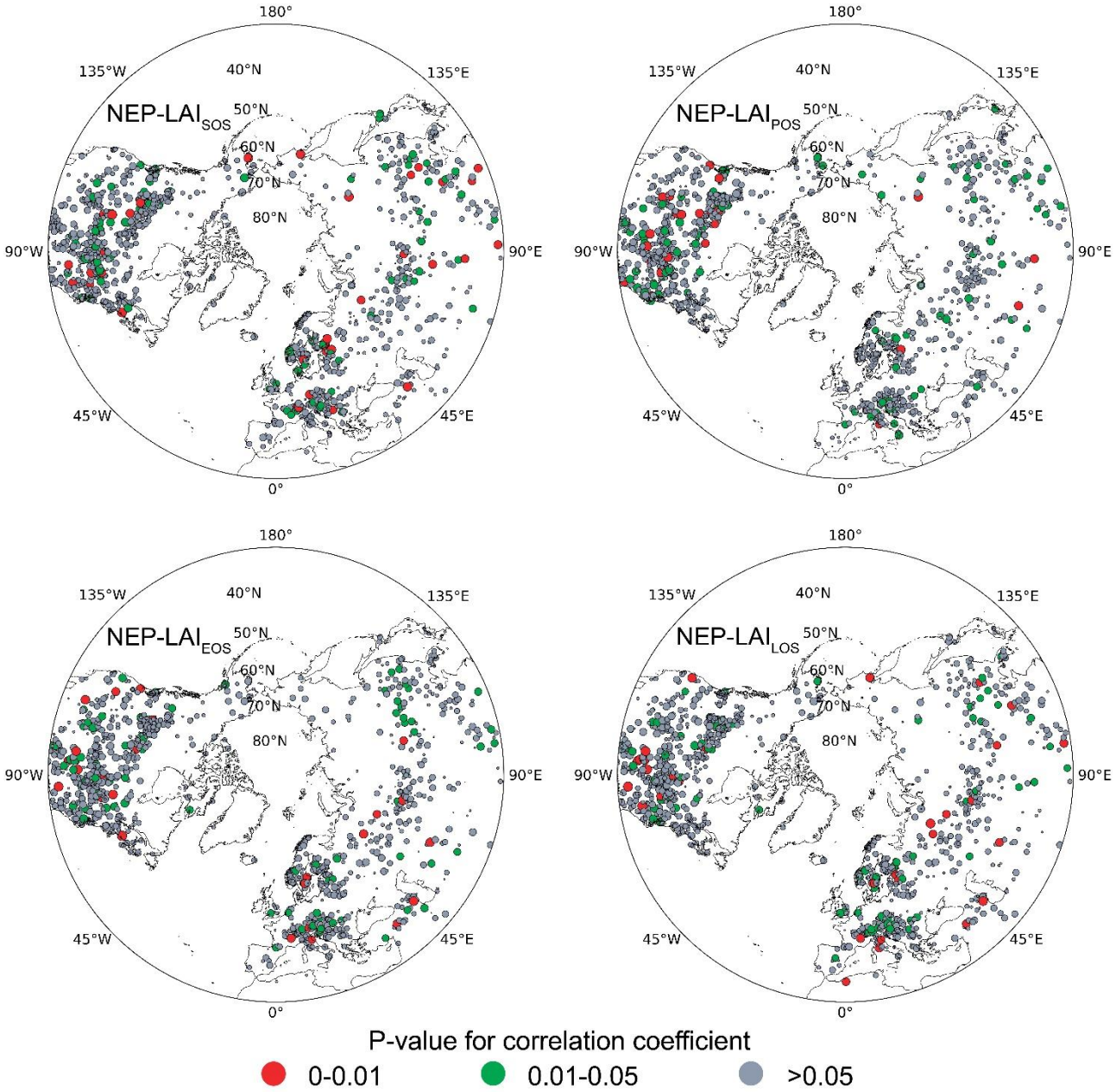


Figure S31: Spatial distribution of p-values for the correlation coefficients between vegetation phenological parameters derived from 500m LAI and NEP at the site scale.

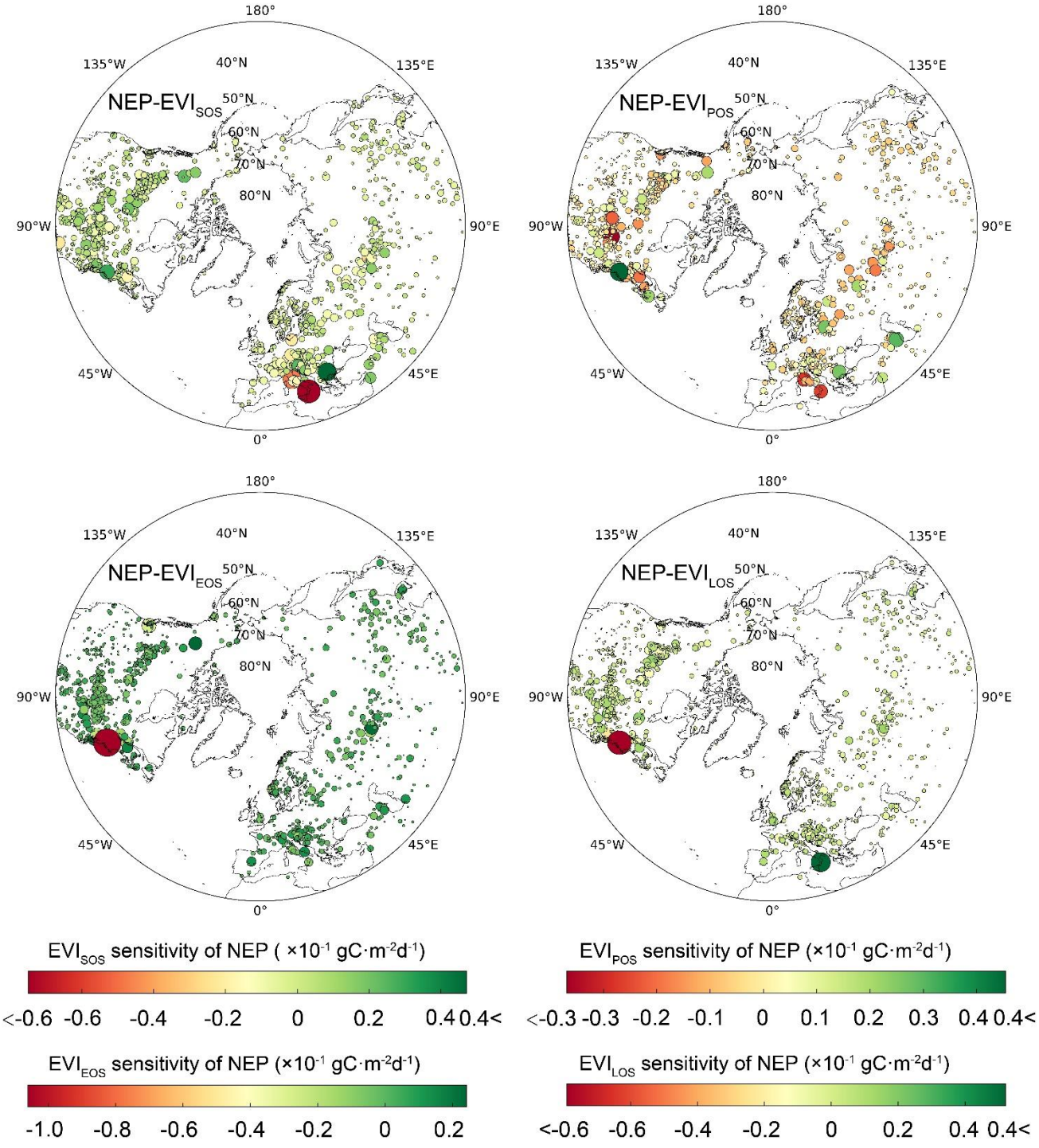


Figure S32: The spatial distribution of the sensitivity of NEP to vegetation phenological parameters (SOS, POS, EOS and LOS) based on the EVI dataset.

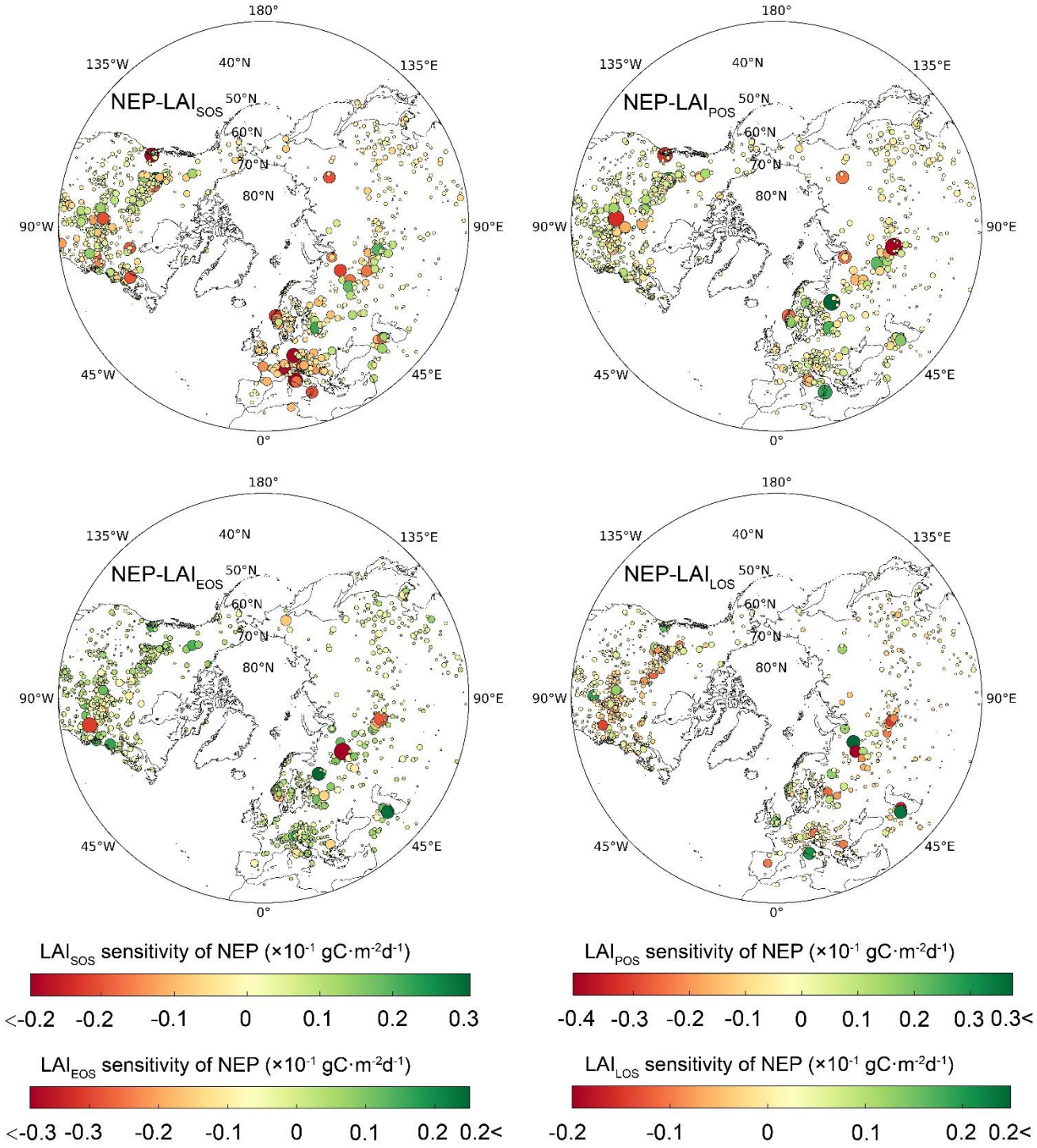


Figure S33: The spatial distribution of the sensitivity of NEP to vegetation phenological parameters (SOS, POS, EOS and LOS) based on the LAI dataset.

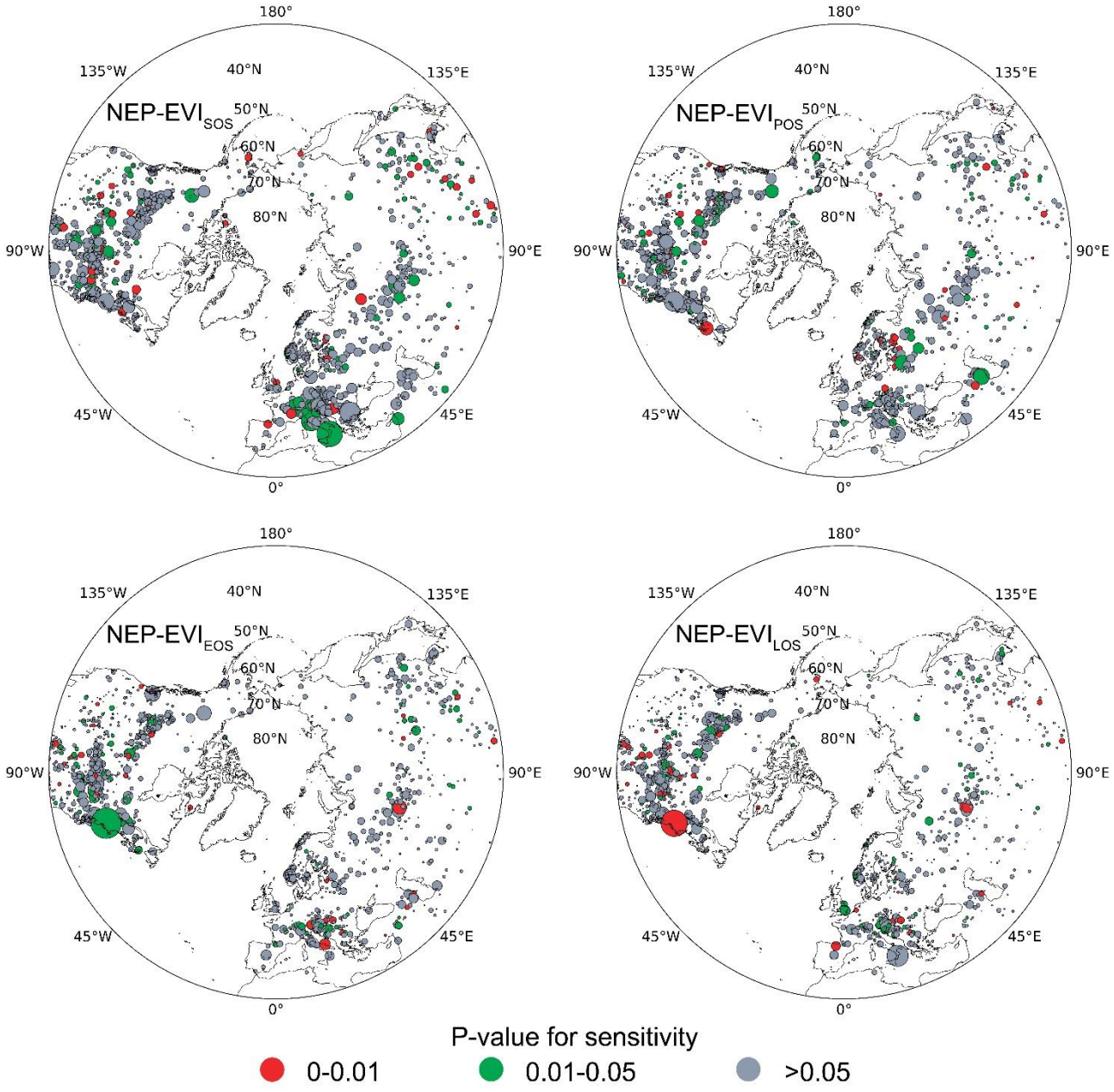


Figure S34: The spatial distribution of the p-values for the sensitivity of NEP to vegetation phenological parameters based on the EVI dataset.

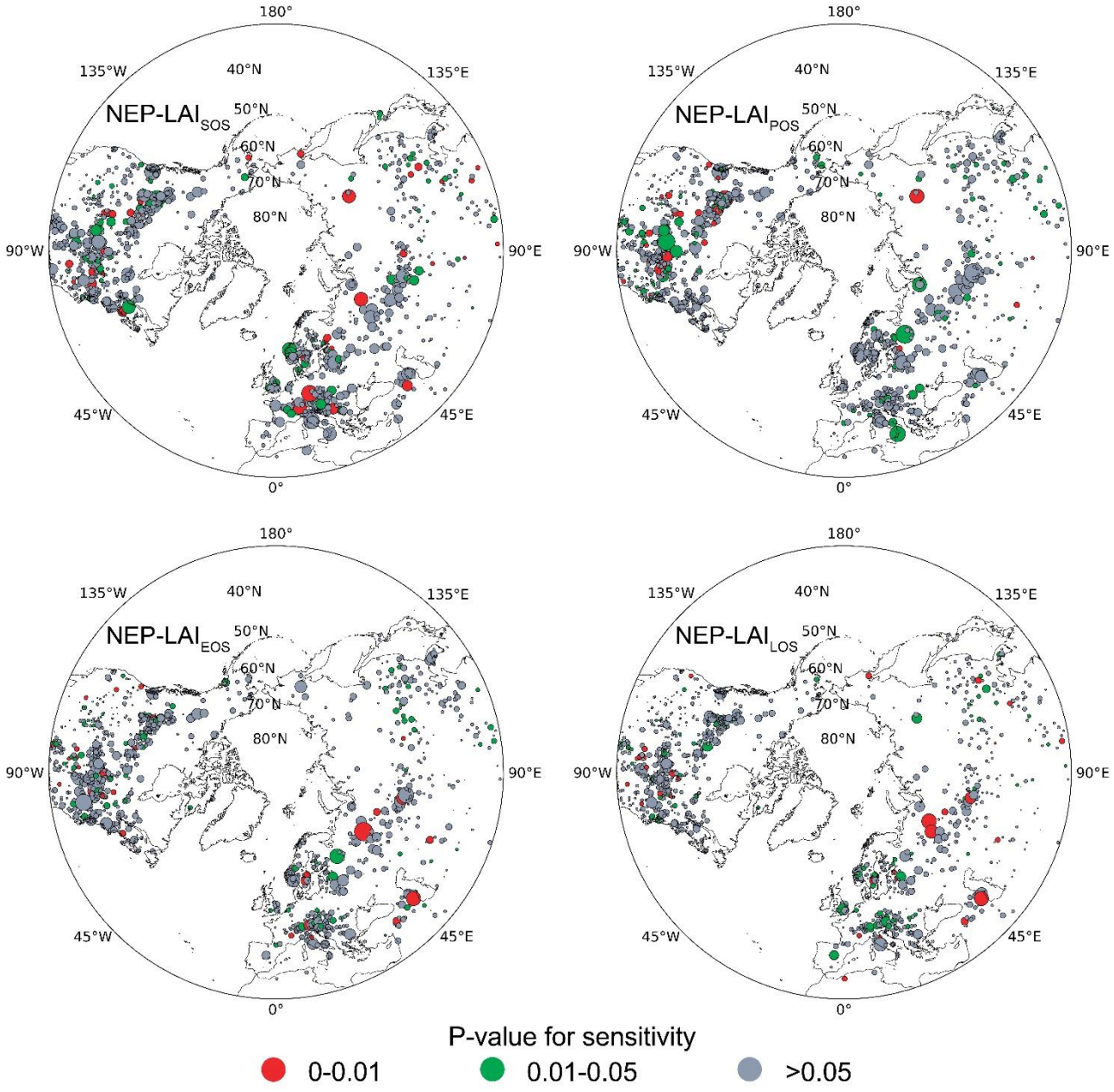


Figure S35: The spatial distribution of the p-values for the sensitivity of NEP to vegetation phenological parameters based on the LAI dataset.

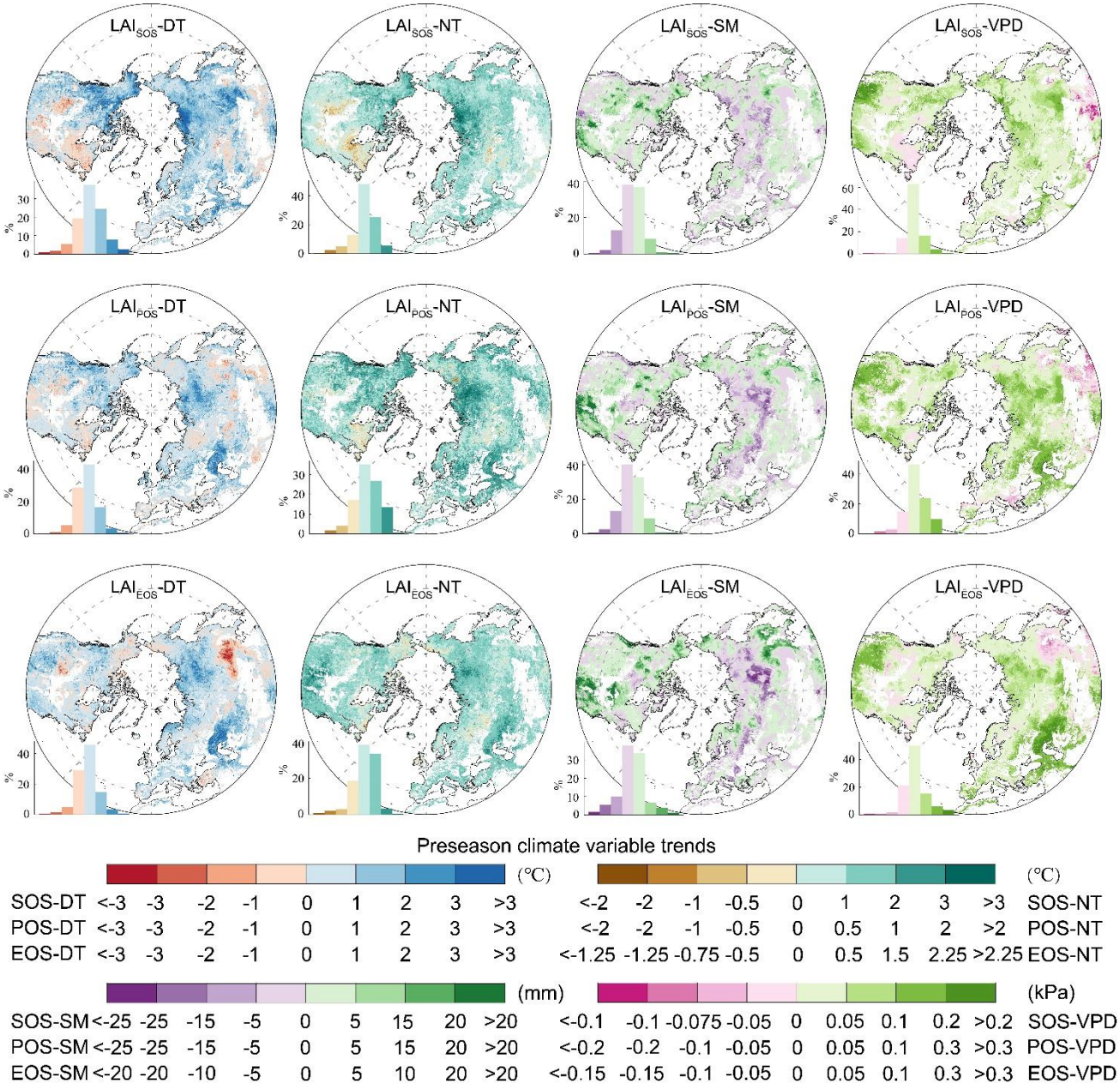


Figure S36: The spatial distribution of the cumulative trend changes of preseason climate factors based on LAI data sources.

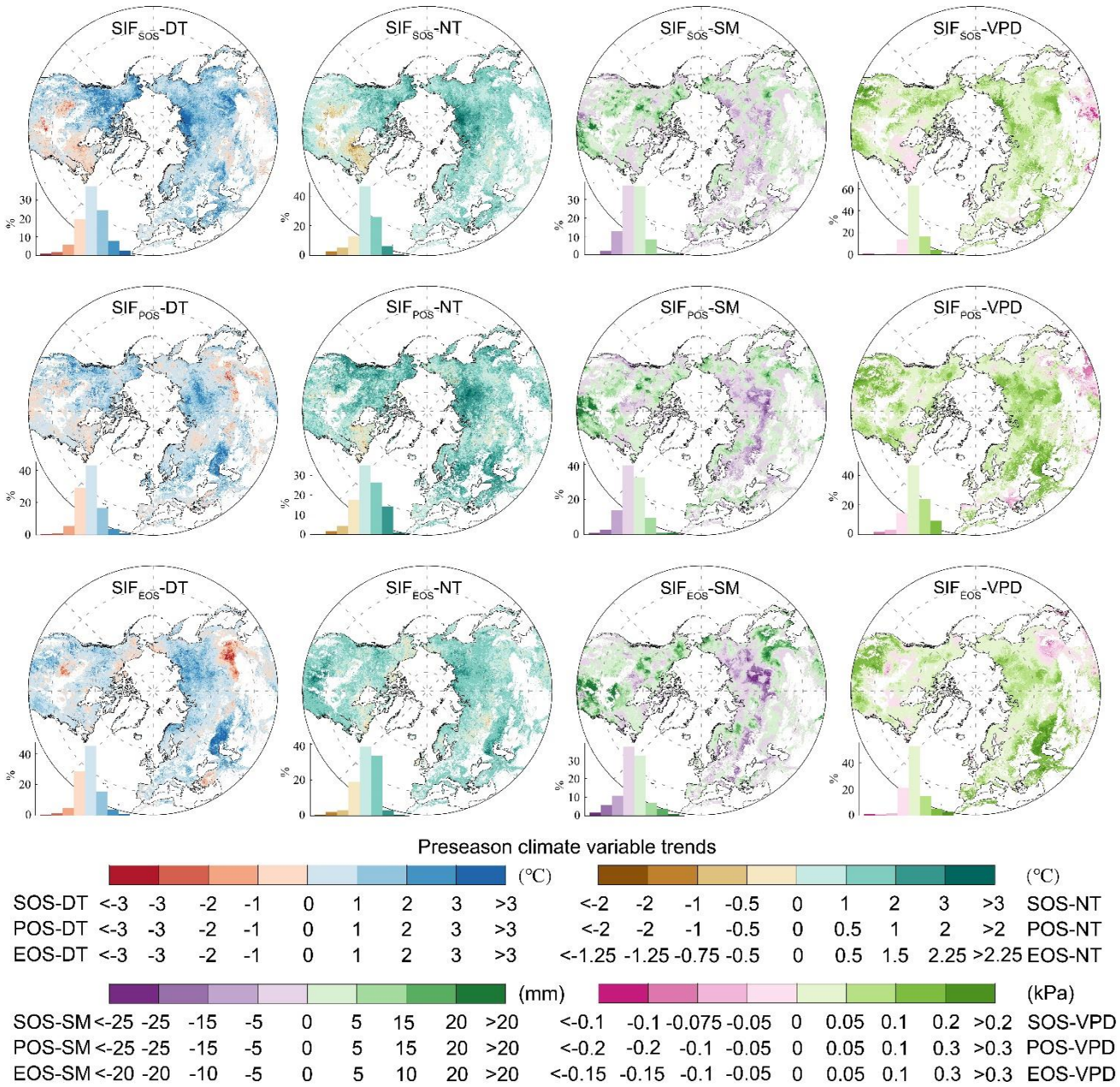


Figure S37: The spatial distribution of the cumulative trend changes of preseason climate factors based on SIF data sources.

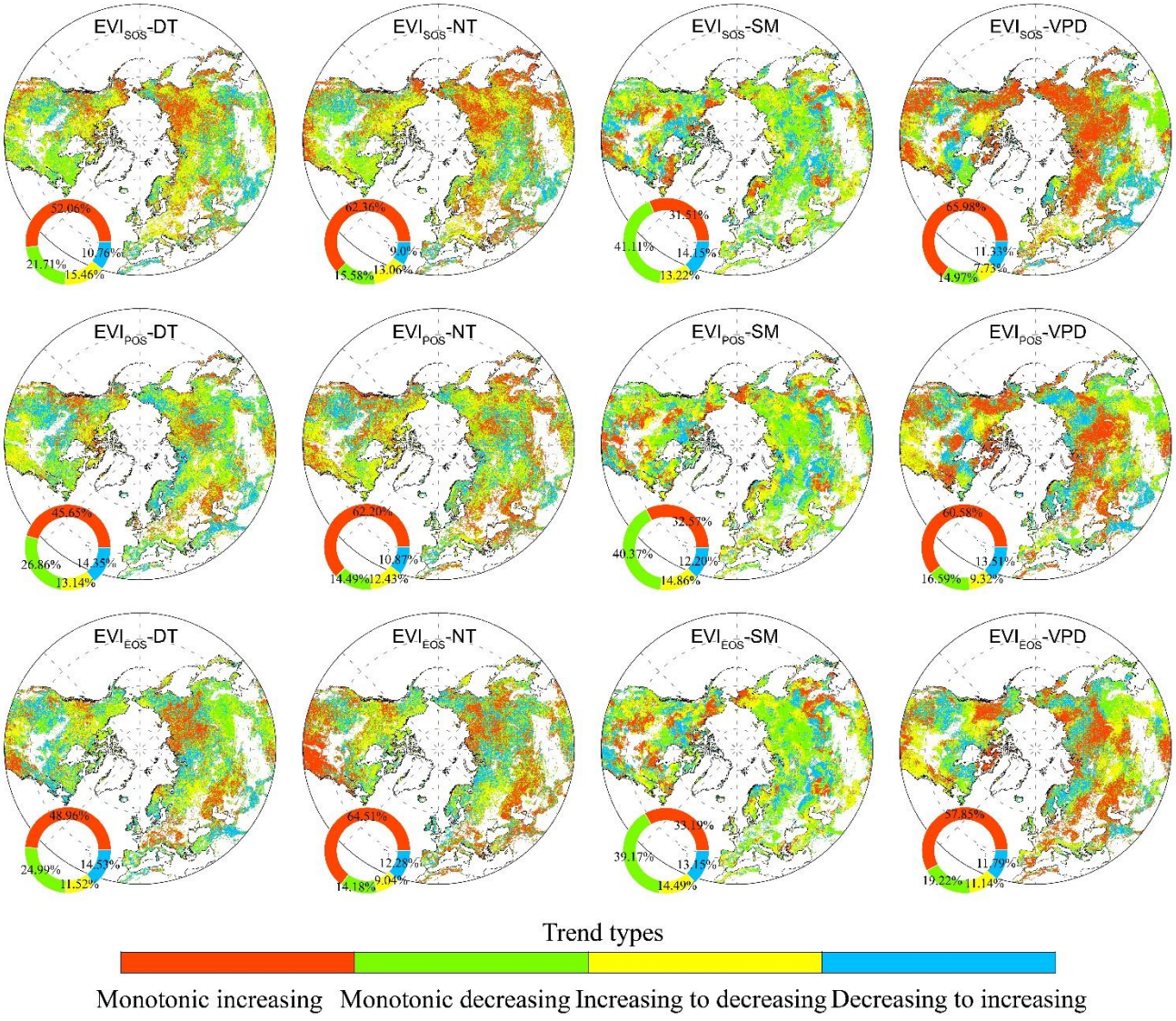


Figure S38: The spatial distribution of trend types of preseason climate factors based on EVI data sources.

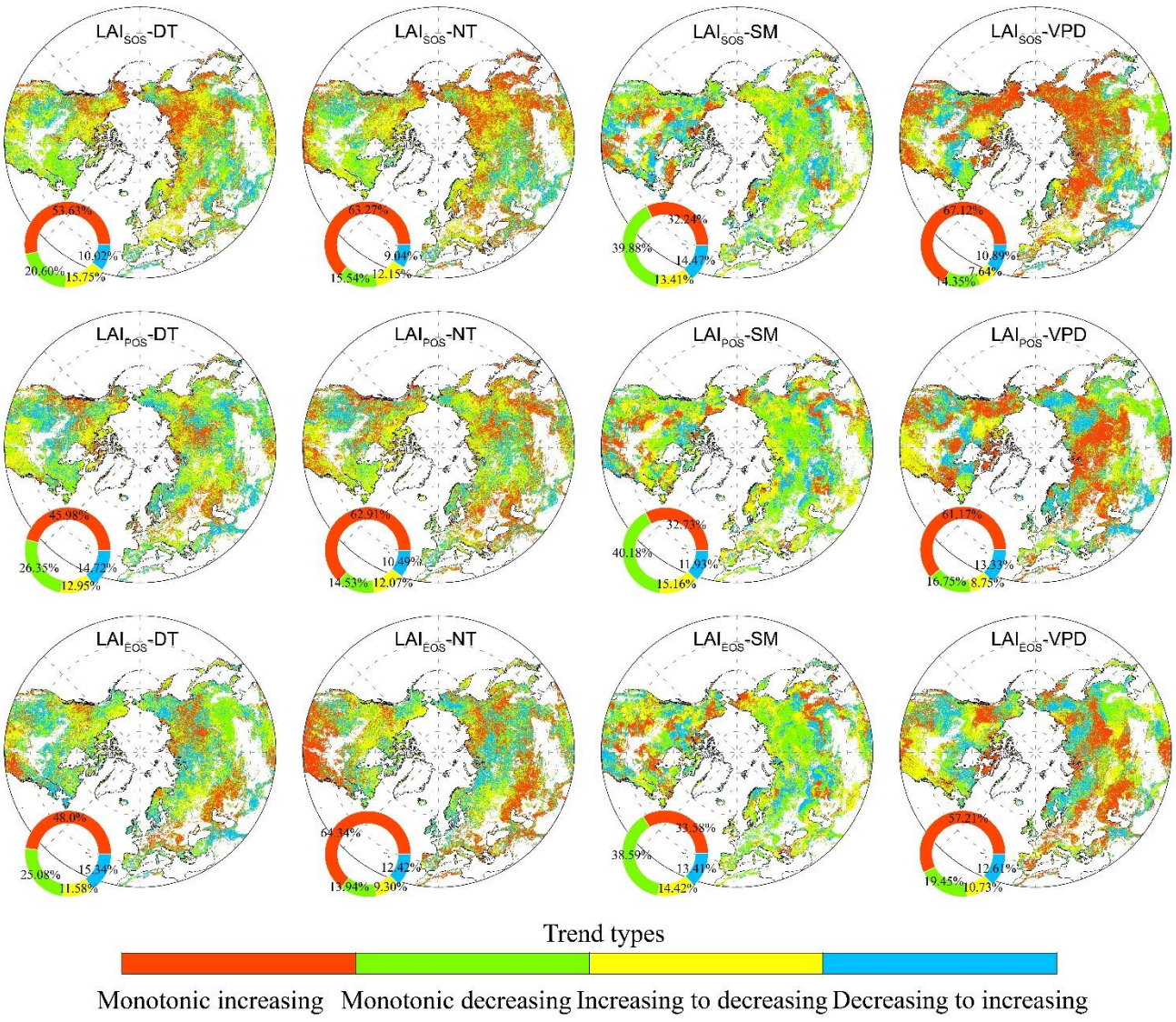


Figure S39: The spatial distribution of trend types of preseason climate factors based on LAI data sources.

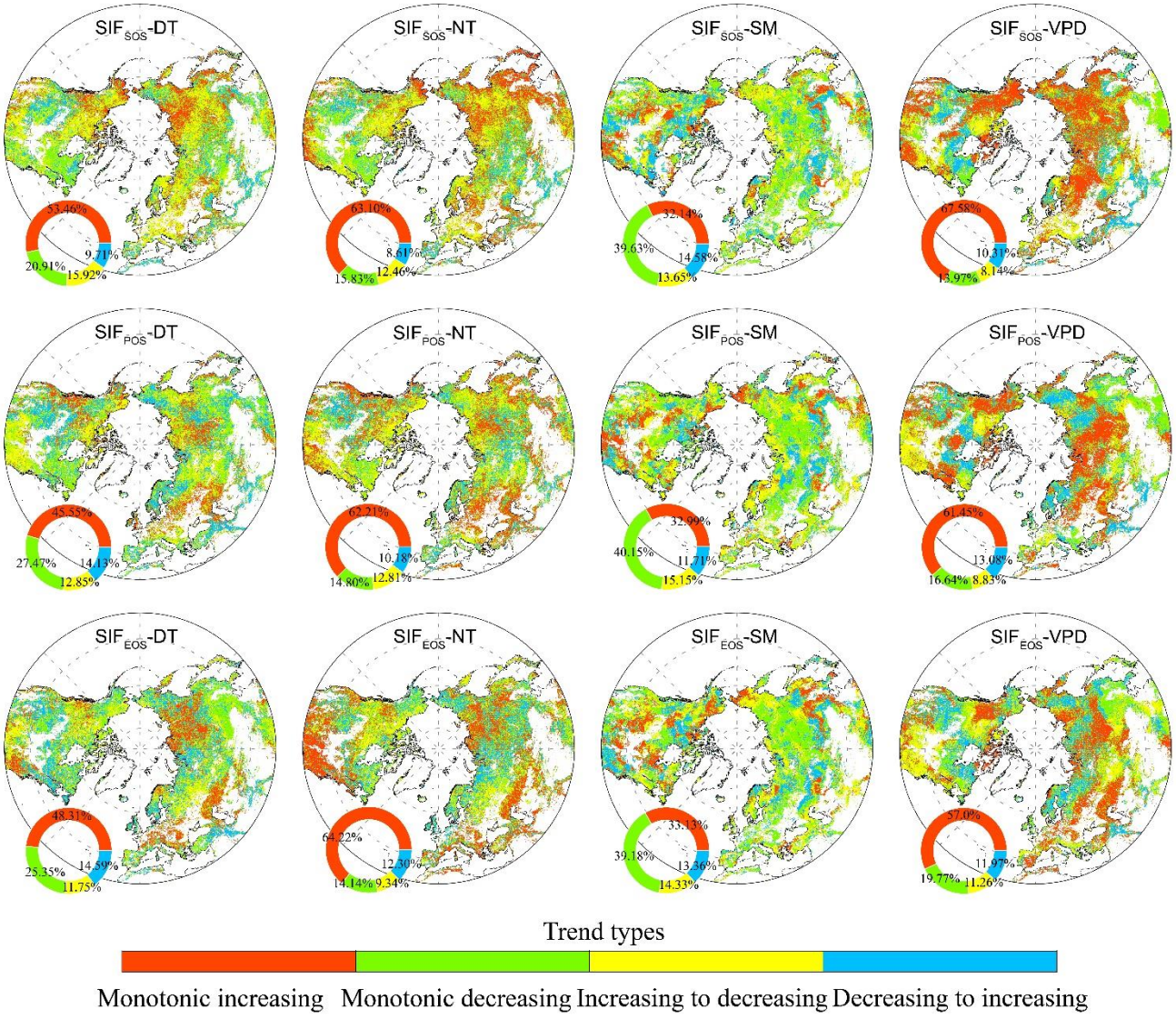


Figure S40: The spatial distribution of trend types of preseason climate factors based on SIF data sources.

Table S5: The percentage of positive and negative pixel statistics for the cumulative trend of preseason climate factors.

Unit: %

Data sources	Climatic factor	SOS		POS		EOS	
		Positive	Negative	Positive	Negative	Positive	Negative
EVI	Daytime temperature	70.96	29.04	63.56	36.44	64.97	35.03
	Nighttime temperature	78.40	21.60	76.04	23.96	75.57	24.43
	Soil Moisture	43.60	56.40	43.70	56.39	44.56	55.44
	Vapor pressure deficit	82.7	17.30	80.09	19.91	75.88	24.12
LAI	Daytime temperature	72.46	27.54	64.11	35.89	64.14	35.86
	Nighttime temperature	79.28	20.72	76.42	23.58	75.43	24.57
	Soil Moisture	46.10	53.90	43.47	56.53	45.38	54.62
	Vapor pressure deficit	83.89	16.11	80.25	19.75	75.32	24.68
SIF	Daytime temperature	72.32	27.68	63.72	36.28	64.62	35.38

	Nighttime temperature	79.25	20.75	76.48	23.52	75.73	24.27
	Soil Moisture	46.96	53.04	43.48	56.52	44.42	55.58
	Vapor pressure deficit	84.36	15.64	80.61	19.39	75.50	24.50

Table S6: The average climate factors and trends of change under different vegetation phenological parameters from 2001 to 2021 in the middle and high latitudes of the Northern Hemisphere.

Data sources	**Climatic factor**	**Annual average (2001-2021)**			**EEMD trends (2001-2021)**			**Slope trends (2001-2021)**		
		SOS	**POS**	**EOS**	**SOS**	**POS**	**EOS**	**SOS**	**POS**	**EOS**
EVI	Daytime temperature (Mean:℃; Trend: ℃ ·yr^{-1})	11.22	19.58	17.36	0.03	0.01	0.02	0.06**	0.03*	0.04**
	Nighttime temperature (Mean: ℃; Trend: ℃ ·yr^{-1})	-0.01	6.94	5.59	0.03	0.02	0.02	0.06***	0.04**	0.04***
	Soil Moisture (Mean: mm; Trend: mm ·yr^{-1})	46.16	35.07	32.80	-0.05	-0.03	0.01	-0.12*	-0.08	-0.08
	Vapor pressure deficit (Mean: kpa; Trend: kpa·yr^{-1})	0.44	0.69	0.62	0.002	0.002	0.002	0.003***	0.004***	0.004***
LAI	Daytime temperature (Mean:℃; Trend: ℃ ·yr^{-1})	7.59	19.13	18.60	0.03	0.02	0.001	0.06**	0.04*	0.03**
	Nighttime temperature (Mean:℃; Trend: ℃ ·yr^{-1})	-3.97	6.36	6.65	0.03	0.02	0.02	0.06***	0.04**	0.04***
	Soil Moisture (Mean: mm; Trend: mm ·yr^{-1})	49.06	35.39	32.41	-0.04	-0.04	-0.04	-0.07	-0.07	-0.05
	Vapor pressure deficit (Mean: kpa; Trend: kpa·yr^{-1})	0.37	0.69	0.66	0.001	0.002	0.002	0.003***	0.004***	0.004***
SIF	Daytime temperature (Mean:℃; Trend: ℃ ·yr^{-1})	7.15	18.75	17.29	0.03	0.02	0.02	0.06**	0.03*	0.04**
	Nighttime temperature (Mean:℃; Trend: ℃ ·yr^{-1})	-3.72	6.53	5.80	0.04	0.02	0.02	0.07***	0.04**	0.04***
	Soil Moisture (Mean: mm; Trend: mm ·yr^{-1})	50.54	37.25	33.14	-0.04	-0.04	-0.05	-0.08	-0.09	-0.08
	Vapor pressure deficit (Mean: kpa; Trend: kpa·yr^{-1})	0.37	0.67	0.59	0.002	0.002	0.002	0.003***	0.004***	0.003***

*Note: The significance levels are represented by symbols (*), where *, **, and *** correspond to significance at the 95% level

(P<0.05), 99% level (P<0.01), and 99.9% level (P<0.001), respectively.

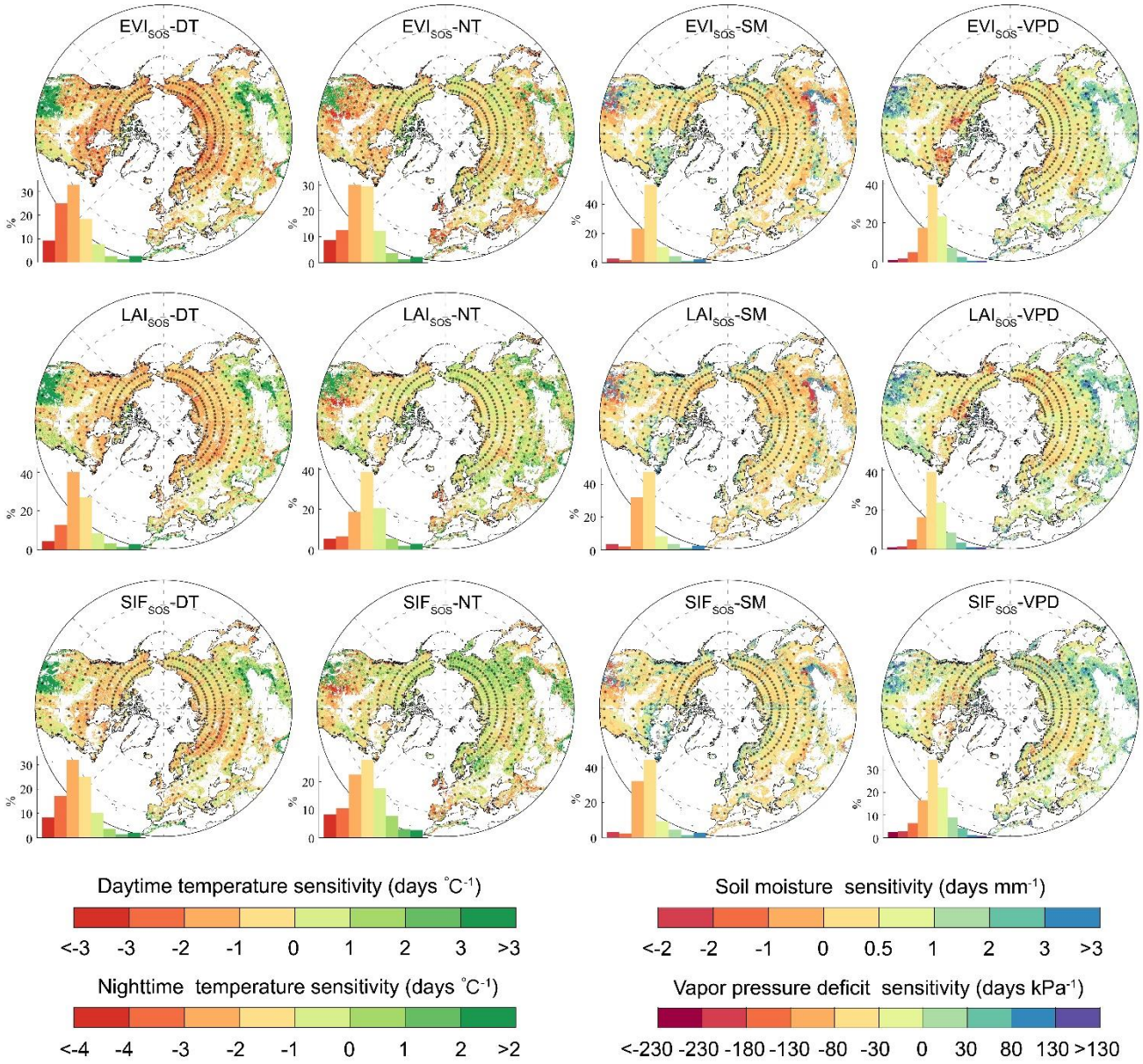


Figure S41: The spatial distribution of the sensitivity of SOS to preseason climate factors.

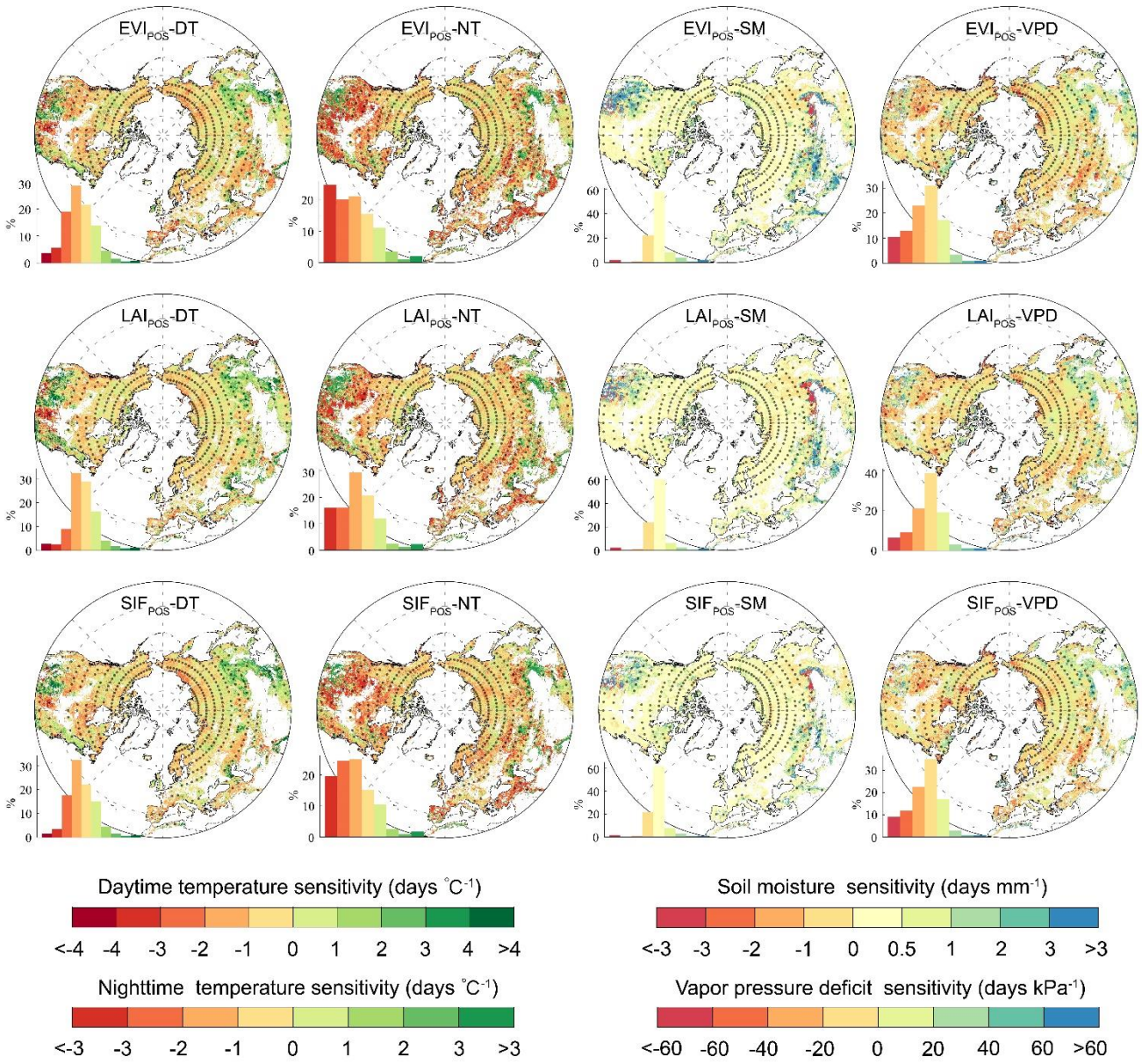


Figure S42: The spatial distribution of the sensitivity of POS to preseason climate factors.

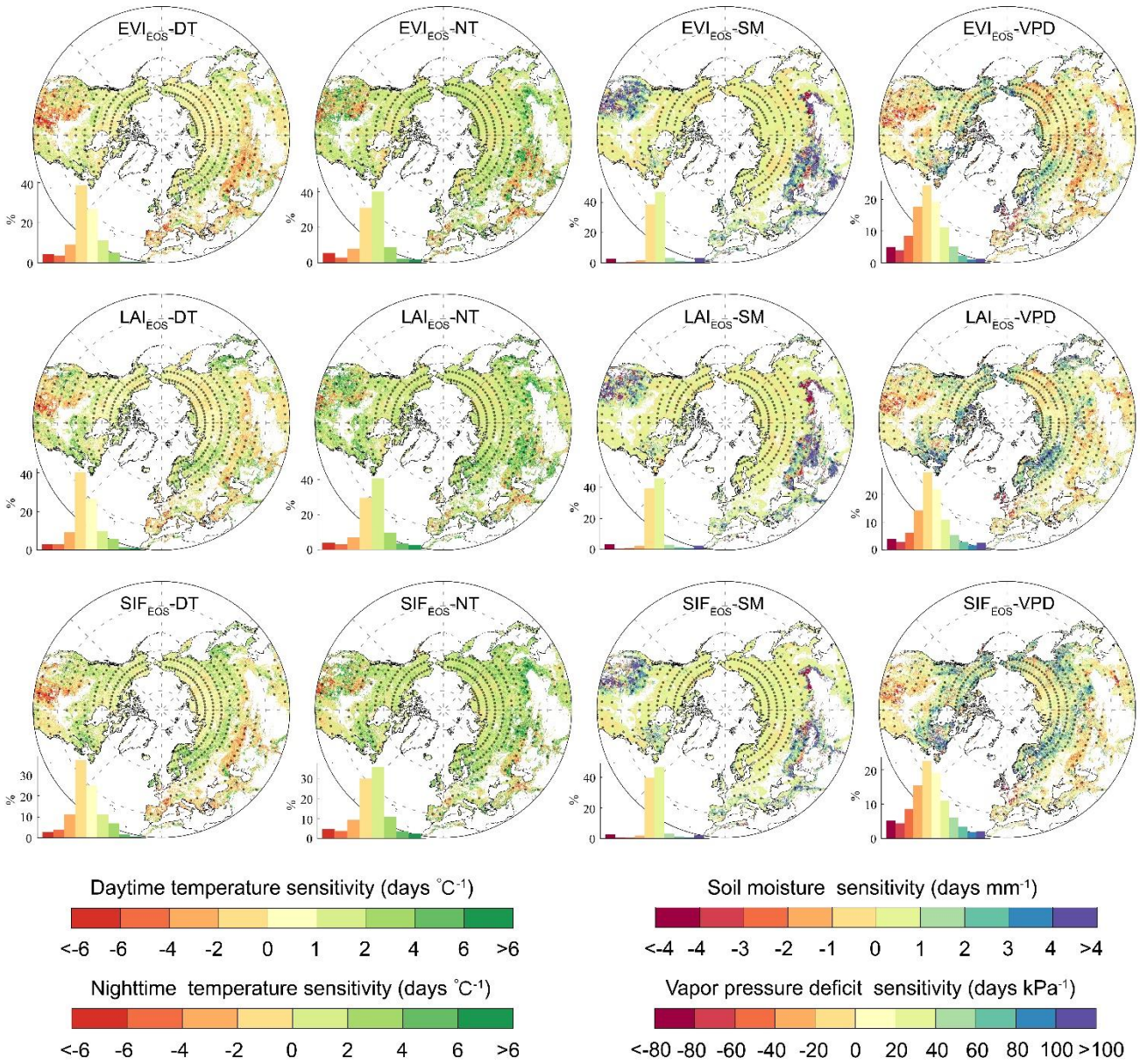


Figure S43: The spatial distribution of the sensitivity of EOS to preseason climate factors.

Table S7: The climate sensitivity of vegetation phenological parameters in the study area.

Data sources	Climatic factor	SOS	POS	EOS
EVI	Daytime temperature (d ℃$^{-1}$)	-1.5703 **	-2.1265 **	-1.8172 **
	Nighttime temperature (d ℃$^{-1}$)	-1.7958 **	-2.9009 ***	-1.851 **
	Soil Moisture (d mm^{-1})	0.3777	0.4346 *	0.2877
	Vapor pressure deficit (d kPa^{-1})	-22.305	-31.480 **	-23.948 **
LAI	Daytime temperature (d ℃$^{-1}$)	-1.5346 ***	-2.0605 **	-0.3832
	Nighttime temperature (d ℃$^{-1}$)	-1.841 ***	-2.4109 ***	-0.02342
	Soil Moisture (d mm^{-1})	0.2952	0.4689 *	0.1014
	Vapor pressure deficit (d kPa^{-1})	-28.966 *	-20.014 *	-3.971

SIF	Daytime temperature (d $^{\circ}C^{-1}$)	-2.0115 ***	-2.7430 **	-1.3068 *
	Nighttime temperature (d $^{\circ}C^{-1}$)	-2.0052 ***	-3.0905 ***	-1.5092 **
	Soil Moisture (d mm^{-1})	0.4567	0.5494 *	0.2705 *
	Vapor pressure deficit (d kPa^{-1})	-44.563 ***	-28.667 *	-16.243 *

*Note: The symbol * indicates significance, and the symbols *, **, and *** represent significance levels at the 95% (P<0.05), 99% (P<0.01), and 99.9% (P<0.001) levels, respectively.

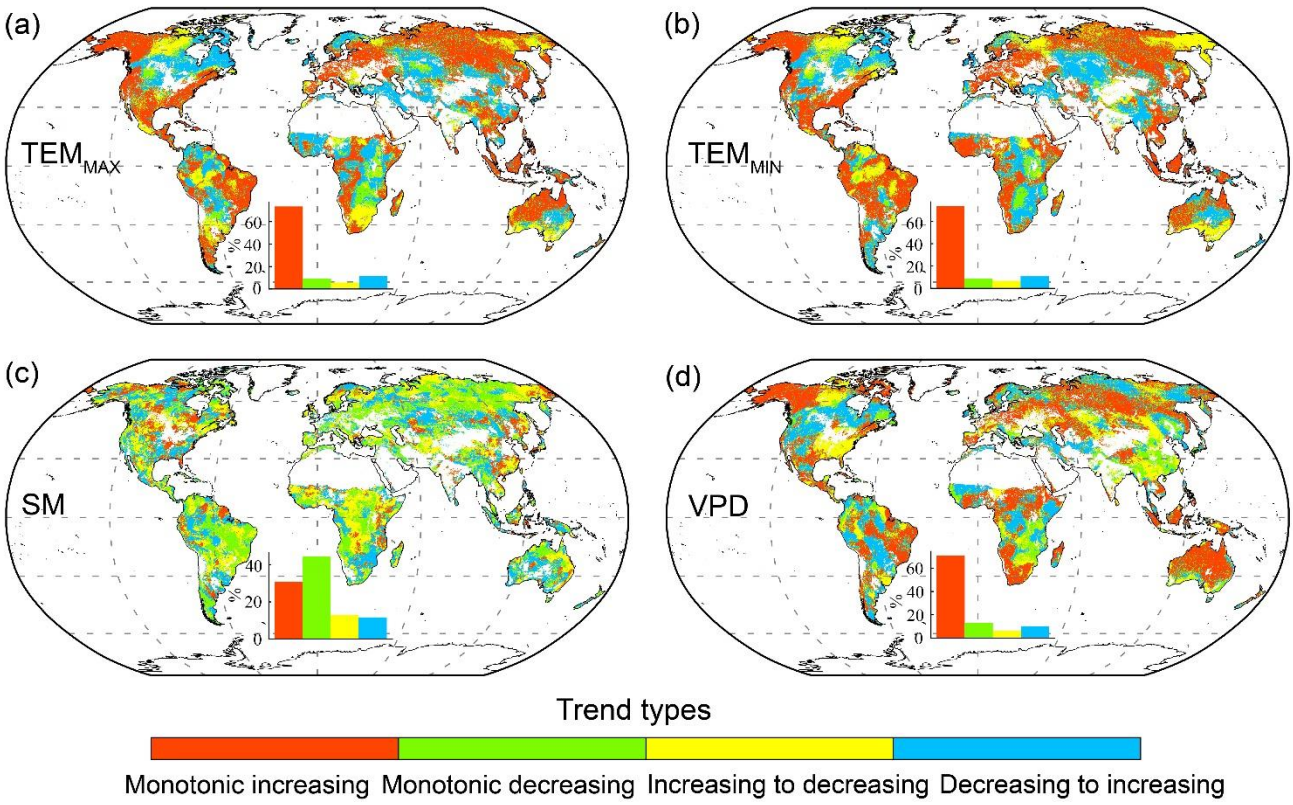


Figure S44: The spatial distribution of trend types of climate factors (maximum temperature (TEM_{MAX}), minimum temperature (TEM_{MIN}), soil moisture (SM), and VPD) based on the EEMD method from 2001 to 2021.